Front. Phys., 2014, 9(3): 398–418
DOI 10.1007/s11467-013-0405-x

REVIEW ARTICLE

Semiconductor nanostructures enabled by aerosol technology

Martin H. Magnusson[1,2], **B. Jonas Ohlsson**[3], **Mikael T. Björk**[2], **Kimberly A. Dick**[1,4], **Magnus T. Borgström**[1], **Knut Deppert**[1], **Lars Samuelson**[1,†]

[1] *Solid State Physics, Lund University, Box 118, SE-22100 Lund, Sweden*
[2] *Sol Voltaics AB, Ideon Science Park, Scheelevägen 17, SE-22370 Lund, Sweden*
[3] *QuNano AB, Ideon Science Park, Scheelevägen 17, SE-22370 Lund, Sweden*
[4] *Center for Analysis and Synthesis, Lund University, Box 124, SE-22100 Lund, Sweden*
Corresponding author. E-mail: [†] *lars.samuelson@ftf.lth.se*
Received September 7, 2013; accepted November 20, 2013

Aerosol technology provides efficient methods for producing nanoparticles with well-controlled composition and size distribution. This review provides an overview of methods and results obtained by using aerosol technology for producing nanostructures for a variety of applications in semiconductor physics and device technology. Examples are given from: production of metal and metal alloy particles; semiconductor nanoparticles; semiconductor nanowires, grown both in the aerosol phase and on substrates; physics studies based on individual aerosol-generated devices; and large area devices based on aerosol particles.

Keywords aerosol, nanoparticle, nanowire, metal-organic vapor phase epitaxy (MOVPE), device physics, light emitting diodes (LED), solar cell

PACS numbers 81.20.Rg, 81.16.Be, 81.07.Gf, 73.63.Nm, 73.23.Hk

Contents

1 Introduction

Mass production of structures with accurate size control has always been one of the central problems in nanoscience. On one extreme, TiO_2 nanoparticles are produced in large amounts but with limited size control [1]. On the other extreme, electron beam lithography (EBL) can produce a low throughput of very small and accurate structures [2]. This discrepancy between precision and throughput can be addressed through self-organization [3] or colloidal chemistry [4], but extreme purity and cleanliness concerns in general make these methods difficult to apply to semiconductor structures; quantum dots grown by metal-organic vapor phase epitaxy (MOVPE) or molecular beam epitaxy (MBE) is a case where self-organization does work for semiconduc-

tors, but is quite limited in terms of size control and choice of materials [5]. Nanoimprint lithography (NIL) is an efficient way to mass-produce nanostructures [6], but due to the complex and expensive stamps, this is often not seen as a flexible method for research.

An aerosol is defined as solid or liquid particles suspended in a gas, and aerosol science and technology has been used since over 60 years, primarily to study the size, shape and composition of airborne particles [7]. The bulk of aerosol science has dealt, and still deals, with natural or man-made ambient aerosols, e.g., cloud formation nuclei, smog, dust or asbestos fibers, with applications in as diverse subjects as climatology, public health and workplace safety [8]. For this purpose, several tools have been developed, which allow scientists to fabricate and precisely classify particles in the micro- and nanometer size ranges according to size, and to measure their concentration in the carrier gas [9]. The aerodynamic properties of nanoparticles depend almost exclusively on their size and shape and only to a small extent on their mass and composition, which means that the same generic characterization and production tools can be applied to a variety of different materials [10].

Due to Brownian motion and other gas-phase mixing and the processes of formation, aerosol particles are inherently random in terms of size and position, and aerosol technology can at best reduce the randomness. Many materials can be produced at very high rates using e.g., flame pyrolysis, and by controlling the nucleation and growth process the particle size distribution can be made rather narrow [11]. Size classification can be performed with very high resolution down to clusters or single ions [12], and for all particle sizes with arbitrarily high resolution [13], at the expense of particle production rate. Positioning of aerosol nanoparticles on a substrate can to some extent be controlled, for example by means of charge patterns in a dielectric [14] or a combination of electrostatics and lithography [15], limited by the resolution of the pre-patterning. Aerosol particles can be deposited as a supersonic jet, which is a serial, low-throughput method with resolution in the μm range [16]. Particles can also be classified by shape [17] and mass [18] as well as by the average aerodynamic diameter.

In this paper, we present a review of 20 years' application of aerosol technology to manufacturing complex semiconductor nanostructures, as well as fundamental physics studies enabled by such structures. The paper is structured thematically and partly chronologically, with four main sections. Section 2 covers the fundamentals of aerosol-based nanometallurgy for making metal nanoparticles, including their applications and the use of metal nanoparticles for modifying bulk semiconductors either structurally or electronically. In Section 3, we describe nanoparticle and nanowire growth directly in the aerosol phase through a unique high-throughput process called Aerotaxy. In Section 4, we describe the development of substrate-based nanowire growth seeded by (Au) nanoparticles, from proof of concept to detailed control of shape and structure, where the Aerosol approach gave the first demonstration of control of size, shape and location of grown nanowires. And finally, in Section 5, we present a selection of key results in nanophysics obtained through the application of aerosol-seeded structures. The bulk of the work has been guided by potential practical applicability as well as fundamental science; where appropriate, we therefore provide references to granted or pending patents based on these technologies.

2 Aerosol-based nanometallurgy

Aerosol technology thus provides an efficient means of producing nanoparticles, the size, shape, and composition of which can in principle be controlled with arbitrary precision. In all the studies covered in this review, a high purity aerosol particle generator was used, inspired by a simpler evaporation/condensation system [19]. Such systems are used in many labs as a simple and reliable source for particles of many non-oxide materials, mainly metals and salts. The tool used in these studies was developed to have sufficient purity to be compatible with semiconductor growth and processing and consists of the following generic components, cf. Fig. 1 (specifics of the actual aerosol system configuration used for a particular study are given in the respective papers included in this review):

1) A carrier gas, e.g., nitrogen, flows through the entire system, carrying the aerosol particles through the various stages.
2) A primary aerosol particle generator, typically a furnace for evaporating metal (a), after which the metal vapor condenses into a dense aerosol of primary particles (b). The generator contains a coagulation zone where the particles aggregate to the desired size range (c).
3) A charging device, whereby the particles acquire a controlled charge distribution, with typically on the order of 10%–20% of the particles receiving a single positive or a single negative charge [20].
4) A differential mobility analyzer (DMA), where charged particles are size selected according to their cross section through aerodynamic resistance in an

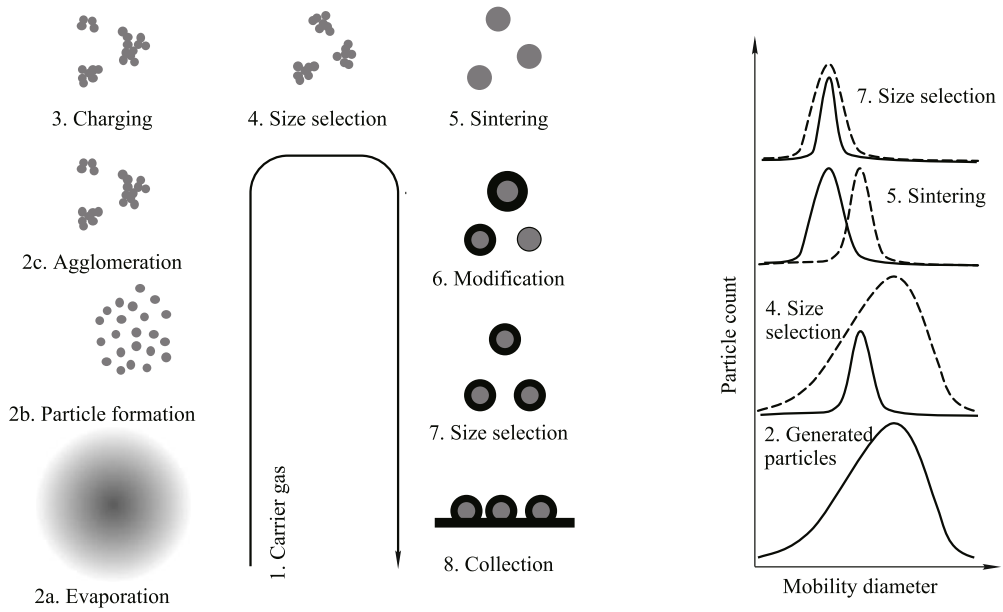

Fig. 1 Schematic representation of the generic steps in aerosol particle or nanowire fabrication. The left sequence illustrates the particle morphology, while the right sequence shows how the process affects the particle size distribution.

electric field [21].

5) A reshaping or sintering step, typically a simple tube furnace, where the particle agglomerates become compact and more or less spherical [23], or to recrystallize, depending on temperature.
6) A modification step, which may involve alloying with another metal (Section 5.2), gas phase reactions (Section 3.1), or gas-phase growth of nanowires (Section 3.2). This step is not used for production of simple metal nanoparticles [23].
7) A second DMA for size selection, which may be used to further narrow the size distribution for nanoparticle production, or to study the change in nanoparticle size distribution due to the sintering or modification steps.
8) A collection stage, where the particles are deposited, e.g., on a substrate or a filter, or sent to an electrometer. Since the particles in general [23] retain their charge, the latter gives a direct measure of the flow of nanoparticles.

2.1 Generation of metal nanoparticles

An important application of the aerosol tool is to produce Au particles between 20 and 100 nm in diameter, which are used for seeding nanowire growth on substrates (Section 4.3). Although simple and reliable in principle, the low vapor pressure of Au requires evaporation temperatures above 1800°C, which leads to high losses due to condensation and thermophoresis as the Au vapor exits the hot furnace. The method can be modified by injection of a precursor gas into the furnace, that upon cracking creates the vapor pressure necessary, which eases the problem with high temperature operations [24, 25]. Figure 2 shows two examples of aerosol-produced metal particles. On the left, Au was evaporated and sintered at different temperatures to make spherical particles [23]. On the right, a chemical precursor, $W(CO)_6$, was thermally cracked to make W particles, which were then sintered at high temperature [24].

Spark discharges are used to create rather pure nanoparticles of graphite and of metals [26, 27]. This method offers a large degree of versatility, making it possible for example to mix two or more different metals [28] since the only condition connected to the material to aerosolize is a certain degree of conductivity. Applications include production of Pd particles for catalysis studies [29] and nanoparticle toxicity [30]. Spark discharges are currently being developed for high cleanliness and for high output of nanoparticle material [31, 32] in the European project BUONAPART-E.

2.2 Controlled alloying of Ga–Au (In–Au) nanoparticles

Alloying Au with Ga, In or Si leads to a eutectic melt, with a (local) melting point minimum at around 60–80 atomic % Au, depending on the alloying elements (e.g. 339°C for $Au_{0.66}Ga_{0.34}$ [33] and 363°C for $Au_{0.81}Si_{0.19}$ [34]. This phenomenon is used for the growth of semiconductor nanowires of silicon and III–V compounds by the vapor–liquid–solid (VLS) mechanism, where the molten

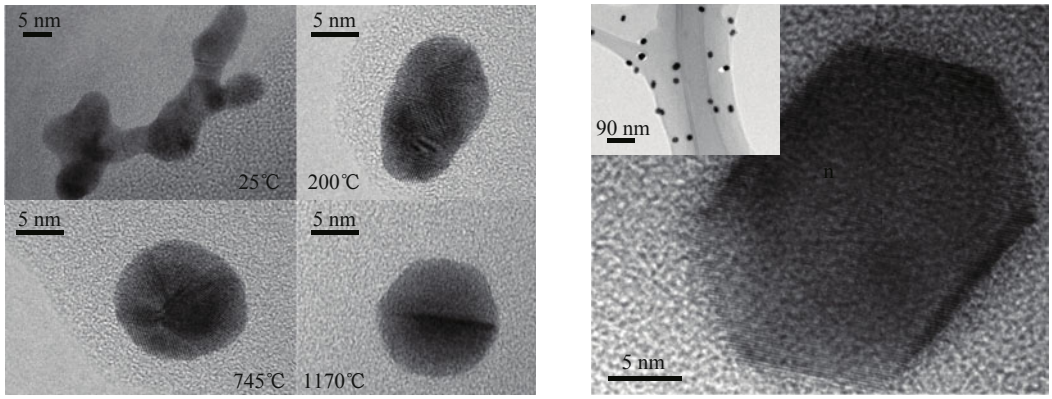

Fig. 2 Examples of metal nanoparticles produced by aerosol technology. *Left*: four TEM images of Au particles subjected to sintering at different temperatures. The initial diameter as selected by the first DMA was 30 nm for the 25°C case and 18 nm for the other three (Ref. [23]). *Right*: a TEM image of a W particle produced by thermal decomposition of $W(CO)_6$ and sintered at 1750°C. The particle mobility diameter before sintering was 25 nm; the inset shows an overview of particles (Ref. [24]).

state of the seed particle is beneficial to the wire growth. In III–V VLS growth, pure Au particles are usually alloyed with the substrate material prior to introduction of the nanowire growth species, or with the growth species prior to wire growth, cf. Section 4.3.

In a study intended to improve nucleation of nanowires, especially for nanotree branches (Section 3.2), Ga was evaporated onto size-selected Au nanoparticles in a simple tube furnace, where the Au aerosol was passed over a crucible containing Ga [35]. It was found that due to Ga incorporation, the particle diameter increased by up to 20 nm, depending on evaporation temperature, and that the diameter increase was independent of the Au particle size. The atomic percentage of Ga could thus be regulated up to 90% for 20 nm initial Au particles (and up to 33% for 140 nm particles), which is sufficient to reach the eutectic melt. Attempting to add more Ga by further increasing the temperature resulted in homogeneous nucleation of small Ga particles, and therefore the Au–Ga particles experienced smaller diameter increase. A study was also performed for the Au–In system with similar results [36].

An alternative method for creating alloyed nanoparticles is to allow for coagulation between size-selected singly charged aerosol particles of two different materials and with opposite polarity, and then selecting only the neutral composite particles [37]. This elegant method can in principle give very good control of particle composition, but suffers from significant losses due to the sequential charging, selection and recharging steps.

3 Semiconductor nanoparticles and nanowires grown in the aerosol phase

In this section, two related methods are presented for creating semiconductor nanostructures directly in the aerosol phase, both named Aerotaxy as a portmanteau of *aerosol* and *epitaxy*. In Section 3.1, the original aerotaxy concept for creating size-selected particles of GaAs and InP is described, and Section 3.2 covers the most recent results on growth of GaAs nanowires from airborne Au seeds. Due to the continuous flow nature of aerosol technology, aerotaxy has the potential of being scaled up to very large volumes, while maintaining a high level of control over the process.

3.1 From size-selected III-droplets to III–V nanocrystals

Motivated by an envisioned application of producing dense layers of quantum dots for lasers or light emitting diodes, the aerosol generator was developed to include XH_3 precursors (X = As, P or N). Starting from a size-selected aerosol of group III metal, adding AsH_3 in a tube furnace, self-limiting transformation of 10 nm Ga droplets into 12 nm GaAs nanoparticles was first demonstrated [38]. The change in mean particle diameter, measured by a second DMA, matched the expected change in diameter from adding an As atom for every Ga atom, cf. Fig. 3. In the first temperature regime up to 200°C, the mean particle diameter remained essentially constant; in the second regime from 200°C to 275°C the reaction is incomplete; the third regime from 275°C to 400°C is a stable plateau where the transformation to GaAs is complete and diameter does not change; and in the third regime above 400°C the diameter again increases due to condensation/deposition of thermally cracked As. Figure 3 shows the change in mean particle diameter as a function of reaction temperature. Transmission electron microscopy (TEM) and energy-dispersive X-ray spectroscopy (EDX) confirmed

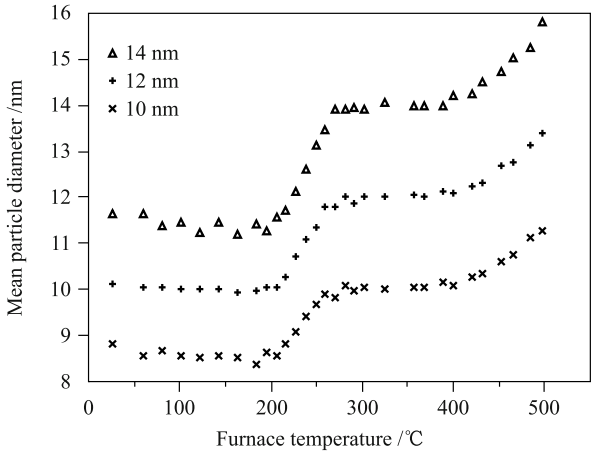

Fig. 3 The mean diameter of particles after the reaction of Ga particles with arsine in a tube furnace at different temperatures, measured in a downstream DMA. Particles with a nominal (as set by the upstream DMA) diameter of 10, 12, and 14 nm were sent into the reaction furnace, the H_2 carrier gas flow was 2 L/min, and the arsine flow was 2.7 mL/min (Ref. [38]).

the stoichiometric composition of the particles.

The aerotaxy method was further used to explore growth of GaN and InN with ambiguous results, and, more successfully, growth of InP [39]. In the latter case, growth from In particles up to 30 nm in diameter was also investigated, with TEM and EDX again confirming the particle composition. The InP particles grown from the larger In droplets were all elongated, with one end thicker than the other, resembling nanoscale tadpoles [40]. TEM investigation revealed that the elongation was always in the ⟨111⟩ direction, the same as for most substrate-grown nanowires as well as for the aerotaxy-grown nanowires in the next section.

3.2 From size-selected Au particles to GaAs nanowires

Semiconductor nanowires, by now, constitute an intensely researched field worldwide, leading to several promising applications. Many such applications do not necessarily require the nanowires to be placed in well-ordered arrays or to be epitaxially rooted in a substrate. In the case of, e.g., light emitting diodes (LEDs) or solar cells, wire ensembles with random placement or short range order would have characteristics very close to ordered arrays, since the wire–wire interference does not contribute strongly [41]. A high degree of control over the wires' crystalline quality, morphology and size distribution is, however, necessary for such devices to perform well.

GaAs and InP nanowires have previously been synthesized without substrates by means of laser ablation, where Ga and As vapor from a solid GaAs target catalytically grows into wires from Au seed particles at low pressure [42], and also analogously for InP [43]. The nanowires made by this method were typically very long and thin, e.g., 3 nm in diameter and 10 μm in length. Liquid phase colloidal chemistry has also been used to make InP wires down to 2 nm in diameter [44], although much shorter. One clear challenge is, however, defined by the ability to produce nanowires with sizes and aspect more suited for optoelectronics, i.e., on the order of 100 nm in diameter and a few μm in length, and with a narrow distribution. By developing the aerotaxy method further, combining aerosol generated seed particles with precursors used in metal-organic vapor phase epitaxy (MOVPE), growth of GaAs nanowires with tunable properties in these size ranges was recently demonstrated [45], cf. Fig. 4. A similar method was previously used to produce carbon nanotubes for which the diameter could be controlled [46].

A fundamental question for nanowire growth has been whether the wire growth direction is determined primarily by the substrate or by intrinsic properties. It is known

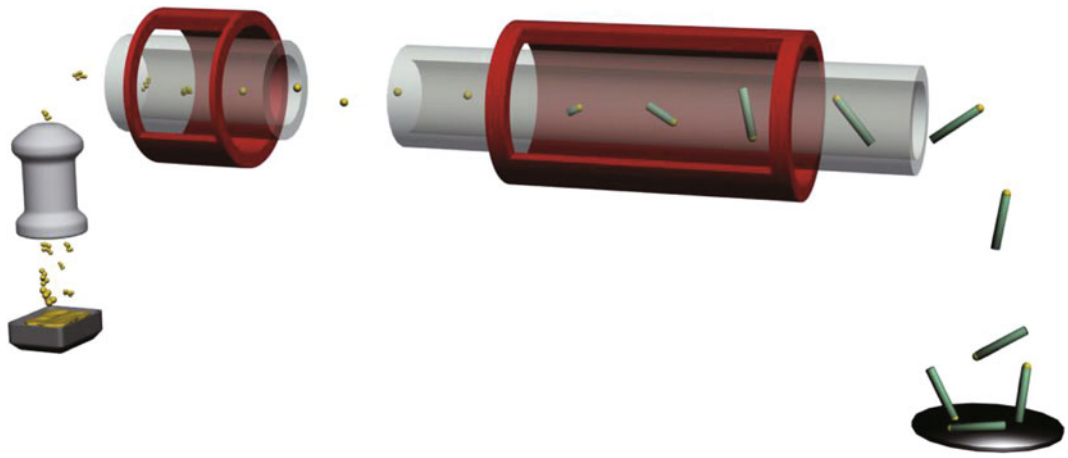

Fig. 4 Principle of nanowire growth by aerotaxy, going from left to right: Au is evaporated, forming an aerosol of Au particles, which are size-selected, sintered, mixed with AsH_3 and TMGa in a tube furnace, and collected on a substrate. In this continuous flow process, 10^9 particles per second grow into nanowires at a rate of 1 μm/s (Ref. [45]).

that on substrates, wires preferentially grow in the group-V terminated ⟨111⟩B direction, but that they can occasionally be made to grow in other directions [47]. In a Gedanken experiment, a Au nanoparticle can be held in free space, while being subjected to a steady supply of, e.g., Ga and As, and then the growth direction of the resulting wire can be determined. One way to realize this experimentally is to grow the wires on an inert substrate, however with unknown interactions with the substrate; another is to keep the Au particles and the growing wires suspended as an aerosol, which is the method we have selected and pioneered.

The aerotaxy nanowire growth takes place in a reactor where a continuous flow of size-selected aerosol of Au particles is mixed with trimethylgallium [$(CH_3)_3Ga$] and arsine [AsH_3]. In the reactor, nanowire growth occurred at a rate of 1 μm/s or faster, and the resulting wires exhibited crystalline quality at least as high as that seen in MOVPE-grown wires at similar temperatures. PL intensities at low temperatures were strong enough to allow measurement on single wires on GaAs without passivation, which indicates the high quality of the materials [45]. Convergent-beam electron diffraction in TEM showed that all the wires indeed grow in the ⟨111⟩B direction; this fundamental property is thus determined at the seed particle–nanowire interface and not by the substrate.

Further development of aerotaxy growth has yielded even better control of the nanowire size and quality, mainly through an improved nanowire nucleation stage and other process conditions, cf. Fig. 5 [48, 49]. The wires do not have the pronounced polycrystalline base seen before [45], and also have fewer twinning defects. The mechanisms behind these effects are currently being investigated. In order to further investigate the mechanisms behind Aerotaxy nanowire growth, an *in situ* TEM growth cell has recently been developed. Here, Au aerosol particles are deposited inside an e-beam transparent cavity made from SiN, together with GaAs powder as source material [48].

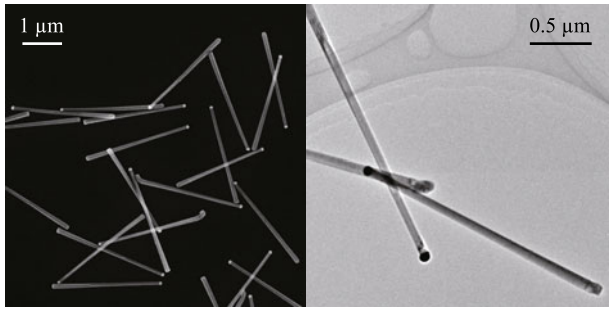

Fig. 5 *Left*: SEM image of nanowires grown by aerotaxy, using 80 nm Au particles as seeds. The wires grow in a tubular reactor at 550°C, with TMGa and AsH_3 as precursors. *Right*: TEM image of nanowires from the same batch, showing a pure zincblende structure and slight tapering extending half way up from the base toward the Au seed particle.

4 Aerosol particles for creating semiconductor nanostructures

Top-down and bottom-up formation of semiconductor nanostructures both rely on one form or another of nanostructures that control and guide the position and shape of the processes. In this part we describe a number of approaches taken where the access to tightly size-controlled nanoparticles are used either as "passive" masking structures or as the active species that provide the origin for the formation of self-assembled nanostructures, such as quantum dots or nanowires.

4.1 Aerosol particles as masks for nanoscale structuring

Top-down transformation of wafers containing thin quantum wells may lead to the re-shaping of the material into ultra-narrow pillars within which each quantum well is now converted into quantum dots confined within the nano-pillars. Ag aerosol nanoparticles were deposited on InP substrates, and used as masks to produce nanopillars by reactive ion etching (RIE) [50]. The substrates contained GaInAs quantum wells, and the envisioned application was to produce a dense array of quantum dots for lasers or light emitting diodes by a cheap masking method. Characterization showed that the pillars/dots were optically active, but that the nanopillars were uneven in shape and exhibited a wide size distribution [51]. They were also too wide for significant quantum effects to occur: 80 nm in diameter, despite the aerosol particles having a mobility diameter of only 40 ± 5 nm. All of these effects were attributed to the uneven shape of the Ag particles, and therefore a sintering step was added to the aerosol process, which improved the size and shape uniformity of the pillars, cf. Fig. 6 [52, 53]. This is an indirect effect of the spherical particles facilitating DMA selection, resulting in a sharper DMA transfer function.

This method for producing nanopillars by use of aerosol defined particles was much more efficient than using EBL, but it did suffer from the same etching process-induced damage to the sidewalls, leading to lower luminescence intensity than what was observed in, e.g., self-organized quantum dots [5]. Metal aerosol particles were at a later stage used for defining seed particles for nanowire growth (Section 4.3), and for making large-scale nanoimprint stamps in silicon [54].

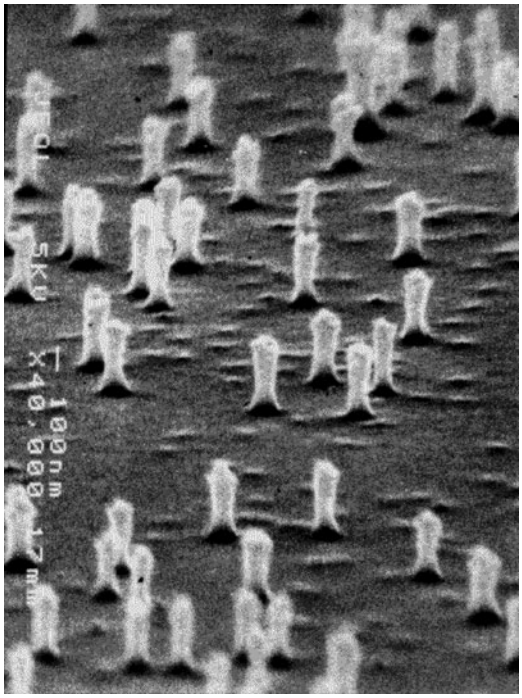

Fig. 6 Nanopillars of InP 100 nm in height and 24 ± 5 nm in top width, made by reactive ion etching using Ag nanoparticles as etch mask (Ref. [53]).

4.2 Aerosol-created QDs on substrates

Although the III–V nanoparticles created by aerotaxy (Section 3.1) were of good crystalline quality as determined by TEM, their photoluminescence (PL) properties were poor, most likely due to non-radiative recombination induced by surface states. This is in contrast to epitaxially grown Stranski–Krastanow quantum dots [5], which self-assemble into dense random arrays during growth of thin layers of lattice mismatched semiconductors, and for which a capping of large-bandgap material provides efficient surface passivation. In order to control dot size and surface density independently, a combination of aerosol and epitaxy was developed, where size-selected group III particles were deposited on a substrate, and transformed into III–V quantum dots using only group V precursors inside an MOVPE reactor [55]; this was inspired by previous work, where metal droplets were formed inside an MBE [56]. By this method, quantum dots of InP, GaN, and InAsP were produced on Si and SiO_2 substrates, actually with reasonably good PL intensities, allowing even single quantum dot PL to be measured at low-temperatures.

4.3 Nanowire growth from size-selected Au aerosol particles

Nanowires are typically defined as quasi-one-dimensional objects with aspect ratios (length to diameter) well in excess of one hundred. The nanowires discussed in this review are crystalline semiconductors, specifically III–V semiconductors, their anisotropy enhanced from growth with metallic particles. The first conceptual model of semiconductor wire growth with metallic particles was suggested by Wagner and Ellis [57] and denoted VLS growth from the three phases involved, vapor, liquid, and solid. Experimental results of Si and Ge "whiskers" were used to substantiate the model. Those whiskers were still in the tens of micrometers down to below micrometer diameters and were grown using chlorine-based chemistry implying fairly high process temperatures. An impressive amount of experiments were performed demonstrating a deep growth control and understanding of growth mechanisms. Even at these large dimensions simple heterostructures of Si and Ge were demonstrated. In the seventies, Givargizov [58], performed equally impressive experiments and demonstrations of whiskers of the same dimensions as Wagner, but in addition Givargizov improved the vapor–liquid–solid model of whisker growth into a theory that is still valid today.

The field of crystal growth of whiskers did not truly advance into the nanometer regime until Hiruma and coworkers working at Hitachi started using MOVPE and size controlled nanoscale Au particles formed by annealing of evaporated thin films to seed growth of III–V nanowhiskers in the early nineties. Hiruma and coworkers expanded on much of the work demonstrated in the sixties and seventies on microscale Si and Ge crystals but now mainly for GaAs and InAs nanowhiskers in the sub-100 nm diameter scale [59]. He also went far beyond that through both fundamental material characterization and through applied physics, proving successful doping to obtain axial pn-junctions in photonic devices and heterojunctions, providing key band gap engineering tools for advanced electronic, photonic, and optoelectronic device applications.

The use of aerosol nanoparticles of (primarily) Au has enabled the early development of nanowire growth on substrates [60], mainly due to the high chemical purity and control of particle diameter. Other methods for creating nanowire seed particles [[6] and references therein], e.g., annealing of thin films, colloids, and EBL suffer from problems with impurities, poor size control, or low throughput.

Nanowire growth catalyzed by Au aerosol particles has been shown to bring several advantages; it allows control of nanowire diameter with narrow size distribution, and, independently, control of surface density. Using chemical beam epitaxy (CBE) to grow GaAs nanowires from such particles, Ohlsson *et al.* demonstrated control over

nanowire diameter and of the position of individual wires [62]. The positioning was done using an atomic force microscope to push Au aerosols on the GaAs surface to chosen locations (cf. Section 5.1). This demonstrated for the first time that nanowires could be deterministically positioned on a semiconductor wafer surface – a key ability needed for practical applications; this was also the first time III–V nanowires were grown from size-selected catalyst particles, cf. Fig. 7.

The demonstration of radial growth control in CBE, in particular suppressing it to zero to achieve taper free wires, made it possible to bring the growth control a step further; changing growth species during growth. In 2002, it was shown that it is possible to switch between InAs and InP in any direction (InAs to InP or vice versa) to form purely axial heterojunctions [63–65]. The heterojunctions formed in that system could be controlled down to the monolayer level, demonstrating InP segments in InAs as thin as 3 monolayers (1.5 nm), cf. Fig. 8. This demonstration, enabled by aerosol gold nanoparticles mediating growth, opened the way for advanced quantum device physics in (quasi-) one-dimensional systems as will be detailed later in this paper. Further study showed that the preferred In/V/Au mix was different under P-rich and As-rich conditions [53]. It was also anticipated that such a ternary mixture would result in a reservoir effect in the particle, leading to a nucleation delay when switching materials in one direction. Such a nucleation delay was indeed observed, and more importantly it was shown that it could be compensated for to facilitate growth of multiple nanometer-thick segments with reproducible thickness [66]. The possibility to switch between group III materials, such as In to Ga in the InAs/GaAs hetero-system, was also demonstrated [67].

One of the elusive challenges of semiconductor technology has been the integration of III–V semiconductors with Si, either for the purpose of integration of optoelectronics and high speed electronics, or, for economic and productive purposes of utilizing Si wafers in III–V technology. Epitaxial growth of III–V material on Si is however a challenge, not only due to lattice mismatch but also by the formation of anti-phase domains (APDs), the crystal requirement being quite intricate: An APD is essentially a crystal region where the column III (A) and column V (B) atomic FCC sub-lattices are swapped in relation to the (A)/(B) lattice of the surrounding zinc-blende III–V crystal; this occurs since the supporting diamond structured Si crystal has two equivalent atomic sub-lattices which can be replaced with either (AB) or (BA) to form a III–V crystal. The method to avoid APD formation in nanowires is to expose only one Si sub-lattice to nucleation of either one of the two III–V sub-lattices [48, 49]. The Si(111) surface is advantageous in this aspect as each atomically flat surface only exposes atomic bonds from one of the sub-lattices, and it also has strong tendency to form double steps. This together

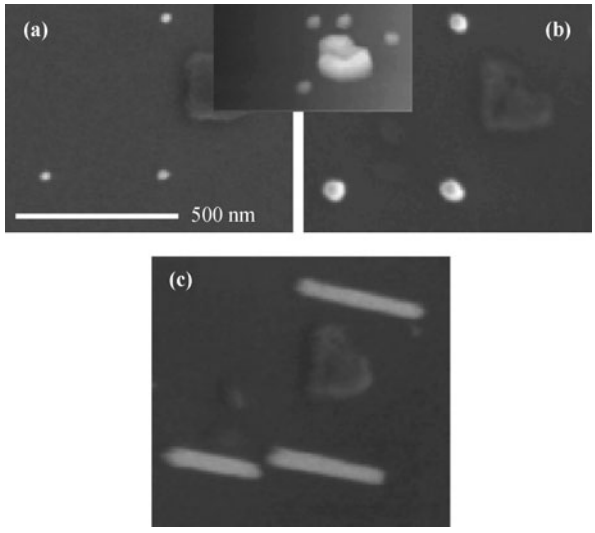

Fig. 7 Positioning of aerosol-seeded nanowires: the top inset shows an atomic force micrograph of an area with an alignment marker and randomly deposited seed particles, measured with the AFM to be 40 nm in height. **(a)** An SEM image of the same area after AFM manipulation of the particles. The particles are arranged as three corners of a rectangle. **(b)** GaAs wires, grown from the pattern of Au nano-particles. Here the increase in diameter due to the alloying step can be seen. **(c)** The same nanowires viewed at an angle of 40°. The wire diameter is close to 50 nm (Ref. [62]).

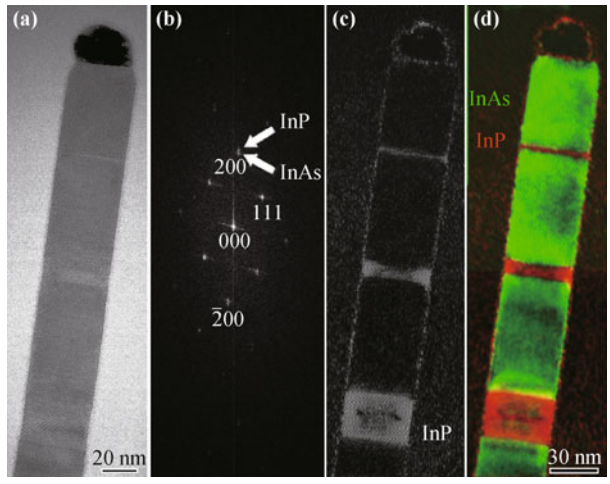

Fig. 8 Composition profile of an InAs nanowire, containing several InP heterostructures, using reciprocal space analysis of lattice spacings. **(a)** High-resolution TEM image of a wire with a diameter of 40 nm. **(b)** Power spectrum of the image in (a). **(c)** An inverse Fourier transform using the information closest to the InP part of the split 200 reflection. InP (bright) is located in three bands with approximately 25, 8 and 1.5 nm width, respectively. **(d)** Superimposed images, using an identical mask over the InP and InAs parts of the 200 reflection, respectively. InAs lattice spacings have been color-coded with green and InP spacings with red (Ref. [64]).

with the preferential (111B) crystal growth direction of III–V nanowires makes for a III–V/Si system with few or no APDs with the potential for wafer production through regrowth of nanowires into epitaxial layers on Si [50, 51]. In 2004, Mårtensson *et al.* successfully demonstrated that Au aerosol particles deposited on Si (111) wafers could give high yield of epitaxial III–V wires, cf. Fig. 9 [68–71]. This technique was further refined to enable nanowire light emitting diodes grown directly on Si substrates, see Section 5.4.

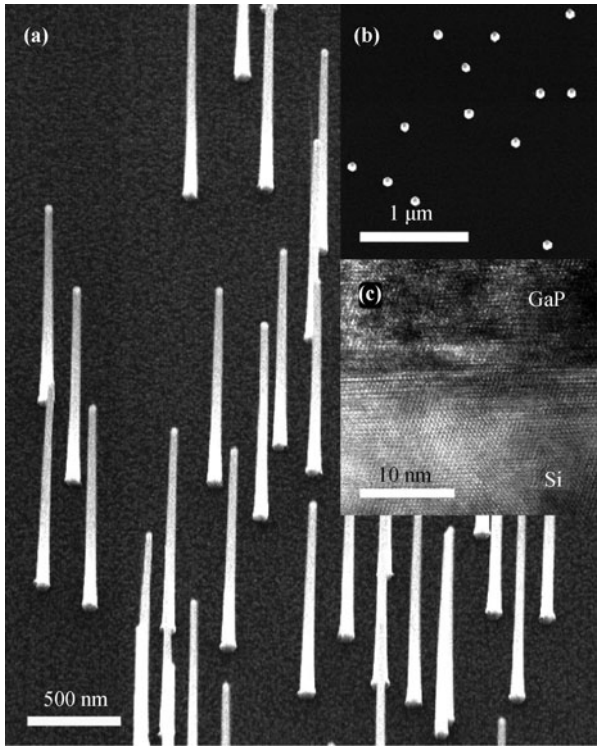

Fig. 9 GaP nanowires grown on Si(111). **(a)** A 45° tilt SEM micrograph of GaP nanowires growing vertically from the Si(111) surface in the [111] direction. The wires were seeded using 40 nm Au nanoparticles. Top wire diameter is close to 40 nm. **(b)** Top view of the same sample showing the perfection in the vertical alignment. Scale bar 1 μm. **(c)** HRTEM image of the Si substrate–GaP nanowire interface. The crystalline direction of the Si substrate is transferred to the nanowire (Ref. [68]).

The ability to precisely, arbitrarily and independently control aerosol nanoparticle diameter and density, together with the highly throughput of this process, have been important for more than simply achieving structures of the desired dimensions. The general understanding of the extremely complex processes involved in seeded nanowire growth has been developed greatly in the last decade, and this development is greatly enabled by size selectivity. As an example, it was demonstrated that growth may under certain conditions proceed from a solid nanoparticle, in contrast to the liquid seed particle required by the VLS mechanism [72]. This understanding was facilitated by size selectively since it allowed for accurate calculation of the volume of gold in the particle. The role of side facet diffusion was also elucidated by comparing nanowires of selected diameters [73]. By exploring nanowire growth using even smaller gold aerosol nanoparticles, it was later determined that the interplay between mass transport and thermodynamic size effects can lead to complex length-diameter relationships [74]. The ability to select and vary nanoparticle size over a wide range, with high throughput and over a reasonably large surface area, is especially critical for studies involving analysis by TEM and related techniques. Aerosol nanoparticles have enabled us to develop an understanding of the size dependence of nanowire crystal structure [75, 76]. Investigations of diameter effects in heterostructure nanowires have also been performed: we have determined that diameter influences hetero-interface sharpness [77] and thermodynamic size effects can play an important role in limiting the minimum diameter of certain heterostructure combinations [78].

One challenge for particle assisted nanowire growth by MOVPE has been the control over axial and radial growth rates. Nanowire growth at temperatures leading to maximum growth rate typically leads to deposition of material on the side facets of the nanowires during the remainder of growth, leading to tapering. In order to promote axial over radial growth, typically a low growth temperature [79, 80] and high supersaturation [81, 82] is used. The general trend in crystal growth however, is that such parameter settings lead to lower quality material [83, 84]. A recent development of nanowire growth allows complete suppression of radial growth for InP [85], InAsP [86], and GaInP [87] as well as InP/GaAs heterostructures [88] by *in situ* use of an etchant, cf. Fig. 10. The method allows for optimization of growth parameters with respect to materials properties instead of mainly morphology, realized for nanowires with diameters from 80 nm [82, 89] down to 15 nm [90] as well as of doped wires [91, 92], necessary for most device applications, cf. Section 5.4. In order to develop a deeper understanding of *in situ* etching, post-growth etching experiments were carried out in which the etch rate was found to be highly anisotropic: etch rates were 100 times more rapid underneath the gold particle than on the sidewalls of the nanowire [89], being opposite to the effect of etching *during* growth. The complete suppression of radial growth was found to be related to pre reactions of chlorinating the group III species before contributing to growth [93]. The chlorinated group III species have bond strengths of several eV, which leads to relatively long surface migration lengths and contribution only to axial

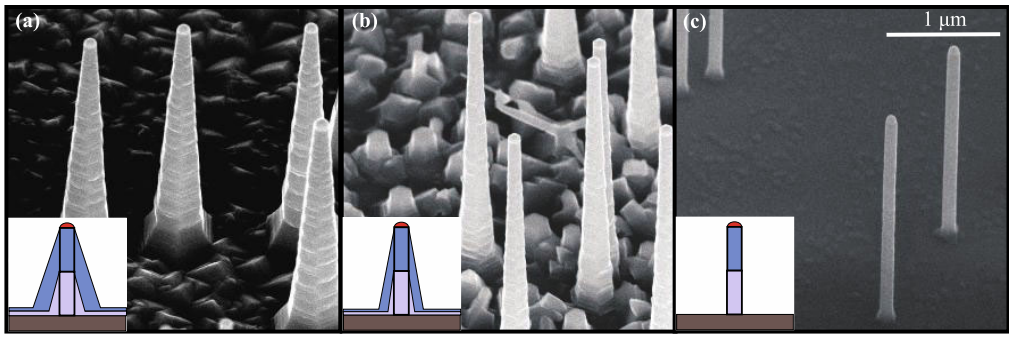

Fig. 10 Scanning electron microscope images of in situ etched InP nanowires. The 80 nm InP nanowires were grown at 450°C with different amounts of HCl in the gas phase: **(a)** reference InP wire, $\chi_{HCl} = 0$; **(b)** $\chi_{HCl} = 1.7 \times 10^{-5}$; **(c)** $\chi_{HCl} = 2.9 \times 10^{-5}$. The images are recorded at the same magnification and at an angle of 45° towards the normal to the substrate. The insets are schematic illustrations of a hypothetical axially defined nanowire component with device functionality sensitive to tapering (Ref. [85]).

nanowire growth by selective decomposition and incorporation via and into the seed particle [94].

4.4 Nano-trees and interconnected tree-nodes as neural nets

Potential applications of nanowire structure are further increased by the potential to integrate them into more complex geometries. There are a wide variety of techniques that yield dendritic or branched nanostructures, in most cases using various self-assembly techniques [95]. A high degree of control over the resulting structure can however be achieved using sequential seeding of multiple generations of nanowires with gold aerosol nanoparticles – yielding so-called nanotrees, cf. Fig. 11 [96, 98]. Aerosol nanoparticles present a unique advantage in fabricating such branched structures, since they can be easily deposited with precise diameter and density control (and even with some degree of control of the distribution along the wires [99]) directly onto pre-fabricated nanowires without damaging the original structure. This technique is highly flexible and a variety of III–V materials (including heterostructures) and growth directions have been demonstrated [95, 96]. We have also demonstrated that branch position along the nanowire access can potentially be controlled [100] and even that interconnected networks can be fabricated using the aerosol seeding technique [101]. This important achievement was based on the fact that for wurtzite nanowires serving as the "trunks", the seeded branches preferentially grow out in specific directions, perpendicular to the original nanowire, which enabled the formation of interconnected networks simply by proper positioning of the original trunk seed particles on the surface.

Control of branched nanostructure fabrication can be further improved by using pre-fabricated alloy particle (see Section 2.2). It is well understood that Au interacts with III–V materials under heating, forming alloys with the group III material and releasing group V material to the vapor. This process can improve nucleation of nanowires on III–V substrates, but can also hinder control of nanowire growth direction and diameter. It also poses a major challenge for growing branched nanotrees, since the "substrate" for branch nanowires is in fact a nanowire itself, and thus limited in volume. For In-containing nanowires (which interact more strongly with Au particles), the result is limited control over the nanowire branch growth. By depositing pre-fabricated Au–In nanoparticles with composition close to the equilibrium composition at growth temperature [35], this interaction between Au particles and nanoparticles can be avoided. We have shown that this technique substantially improves the resulting nanotree morphology [102].

5 Aerosol-enabled nano-physics and devices

As discussed already in Section 4.1 the tight control of the size distribution of aerosol-fabricated nanoparticles offers tools to create designed and functional materials and devices. In this section, dealing with phenomena related to device physics, we describe four special such sub-areas, one (i) where the small size of the metallic aerosol particles enables Coulomb-blockade devices to be designed and realized, one (ii) where the rectifying, Schottky-like interfaces between such aerosol particles can be used to induce electronic functionality for contact formation and to produce semi-insulating materials, one (iii) with the very rich physics studies of quantum systems formed in aerosol particle-induced nanowires, and, finally, one (iv) describing the realization of electronic and optoelectronic devices from aerosol particle-grown

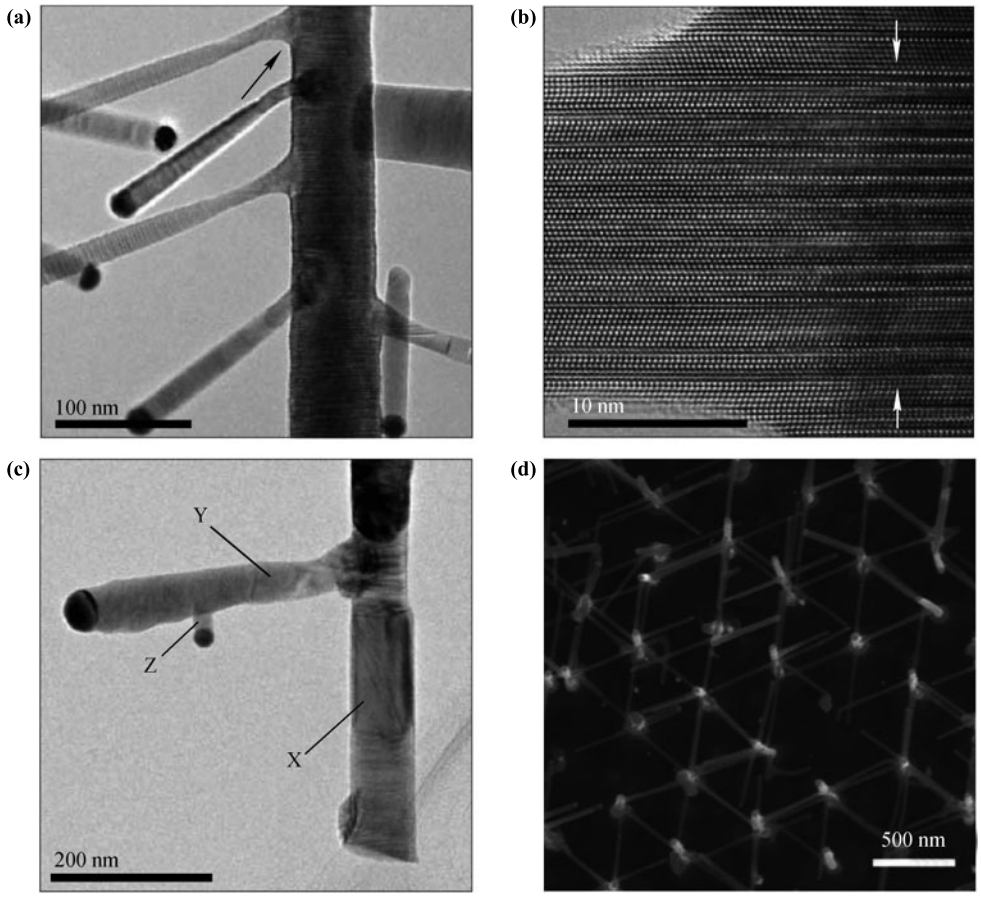

Fig. 11 Nanotrees made by growing nanowire trunks from Au seed particles, deposition of Au or Au-In aerosol particles, which end up on the trunks, and subsequently growing nanowires again (Ref. [96]). **(a)** Image of a trunk exhibiting five branches, with three different growth directions visible. The position of (b) is marked by an arrow. **(b)** Branch-trunk interface (indicated by arrows) at higher magnification. The horizontal bands of alternating wurtzite or sphalerite structure continue smoothly out into the branch, with no apparent interface region in the crystal. **(c)** Image of three-level growth showing the trunk (X), branch (Y) and leaf (Z). The morphology of each level is controlled by growth parameters. **(d)** SEM image of a network of nanotrees with trunk positions defined by EBL, the hexagonal alignment of which ensures that branches will hit neighboring trunks (Ref. [101]).

nanowires.

5.1 Aerosol nanoparticles as functional SET-objects

Ultra-small metallic nanoparticles are interesting as Coulomb islands, where the very small capacitance leads to charging energies that can be larger than kT, at least at fairly low temperatures. Atomic force microscopy (AFM) was employed to characterize the nanopillars described above. However, when used to image the aerosol particles, it was found that the AFM tip, when used in contact mode, very efficiently moved the particles on the surface [103]. A highly accurate method to arrange nanoparticles on a substrate was developed using this effect: image the nanoparticles in non-contact mode, lower the tip to move a particle, and then image the new configuration, cf. Fig. 12 [104]. Apart from allowing precise positioning of small objects and enabling nano-electronic studies, it also allowed us to use the AFM to accurately measure the size of the nanoparticles, far below the resolution of the AFM tip, something that was

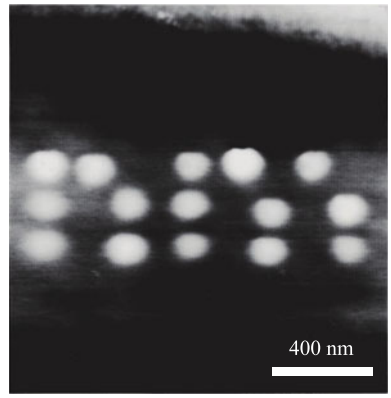

Fig. 12 The letters "nm" written with 30 nm GaAs nanoparticles using an atomic force microscope (Ref. [104]).

very difficult to acheive before; tip convolution effects in AFM make lateral measurements less accurate than vertical. The particles were in this case made from GaAs, produced by aerotaxy, see Section 3.1. The AFM method was employed to create atomic-scale point contacts between EBL-defined Au discs [105], and also for positioning Au nanoparticles for nanowire growth [62].

Nanoparticles of non-noble metals can be expected to partly oxidize when exposed to air, but this process was assumed to be slow enough to allow measurements before the particle oxidized completely. With a well-controlled oxidation of a thin surface layer of the aerosol particle, in the range of few nm, this approach can provide a self-assembly of the combination of the metallic Coulomb island and the thin oxide functioning as the tunnel barrier. Indium was chosen as the base metal particle for which the formation of a thin insulating oxide is easy to control. This would then provide us with a simple way to produce a single electron transistor (SET), by squeezing the In particle between Au discs. A Coulomb gap of 50 meV was indeed measured in the particle, with clear signs of Coulomb blockade measureable up to almost 200 K, cf. Fig. 13 [106]. Further SET studies employing AFM for manipulating particles into the desired place include the realization of an SET with an island consisting of an 8 nm Au aerosol particle with carbon nanotube leads [107] and of a Au disc double dot SET [108, 109].

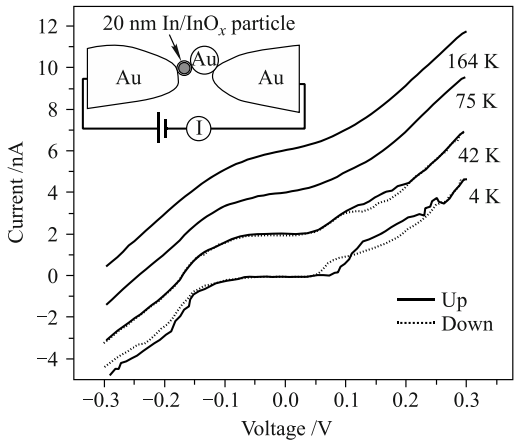

Fig. 13 Current–voltage characteristics of a Coulomb blockade device made from an In aerosol nanoparticle between Au contacts (see inset), recorded at different temperatures. The curves are offset by 2 nA along the current axis for each of the higher temperatures, and both the upward and downward sweeps are shown. The Coulomb gap is 50 meV, and is visible above 150 K. The hysteresis and random fluctuations at lower temperature is attributed to charge trapping in the InO_x shell (Ref. [106]).

5.2 Aerosol nanoparticles for designed electronic functionality

Metallic aerosol nanoparticles can be used as a novel way of locally modifying the electronic properties of bulk semiconductors. This proved to be a both efficient and scalable method in cases where the details of local effects are less important than the average density, similar to the random placement of dopant atoms in a crystal lattice.

Silicon carbide (SiC) is an important high-current and high-temperature semiconductor. In order to achieve low resistance contacts to SiC, Au nanoparticles [23] with 20 nm diameter were deposited with a surface density of 90 μm^{-2} on the substrates, and then covered with a 200 nm thick Ti contact. This contact provided a significant lowering of the Schottky barrier height (SBH) on n-type 4H and 6H SiC, with no degradation of the Schottky diode ideality factor [110], while the effect was smaller on p-type material. The effect was efficiently explained with a simple dipole layer model, where the electric field was enhanced on the rim of each nanoparticle due to the large difference in SBH between Au and Ti.

Semi-insulating material, like GaAs and InP, are preferably used as substrates for electronics applications operating at very high frequencies and where any coupling between devices via the substrate must be avoided. For GaAs such semi-insulating material has been realized by the deliberate incorporation of high concentrations of mid-gap deep levels, as obtained under very high V/III ratios during fabrication, and most likely related to As_{Ga} anti-sites. It was also speculated on whether small inclusions of As-clusters might give rise to internal depletion, where such clusters might act as nano-scale Schottky barriers. In previous studies [111] we had proposed to create buried nano-scale Schottky-barriers formed in the interface between metallic particles and the surrounding material. For sufficiently tightly positioned buried nanoparticles the depletion regions will overlap, thus providing insulating properties. It had previously been shown that the conductivity could be changed over 7 orders of magnitude inside epitaxially grown GaAs containing embedded EBL-fabricated 50 nm wide tungsten discs [111]. Applications of W overgrowth included permeable gate [112] and resonant tunneling transistors [113]. In order to more rapidly cover large surfaces with even smaller nanostructures, W aerosol nanoparticles with 20 and 30 nm diameter [24] were deposited with surface densities up to 200 μm^{-2}, yielding a tunable increase in resistivity of up to 500 times, cf. Fig. 14 [114]. Also in this case, simple theory assuming bulk SBH explained the results appropriately, but the randomness of the aerosol particle positions gave a higher conductivity than what would be expected from, and observed for, equidistant particles [111].

Other examples of electronic devices based on aerosol

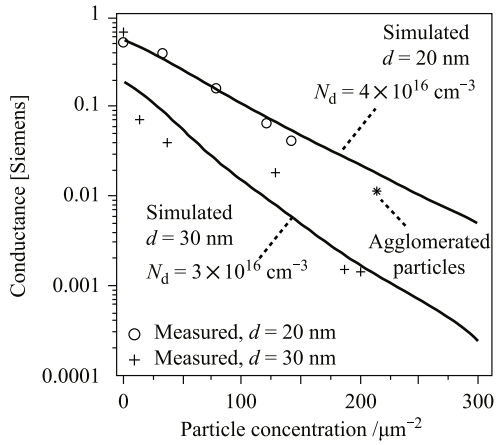

Fig. 14 Semi-insulating GaAs made through incorporation of W aerosol nanoparticles: experimental conductance results for two particle sizes, with lines showing the expected conductance based on a simple Schottky depletion model. The measured point marked "agglomerated" indicates the effect of particle agglomeration for d = 30 nm (Ref. [114]).

nanoparticles include a floating-gate memory with silicon nanocrystals [25], and gas sensors made from SnO_x, In_2O_3 and PbS nanoparticles [115, 116]. For these and other applications, semi-structured deposition of particles directly from the gas phase may be advantageous, which can be achieved by inducing a pattern of electrical charges and allowing the nanoparticles to settle on, or be repelled by, the charged areas. In this way, a resolution better than 100 nm is possible, although the position of individual nanoparticles cannot be controlled exactly [14, 117].

5.3 Nanowire-based physics

The main applications of substrate-grown nanowires have been for studying phenomena in nano/quantum-physics, and (more recently) for developing functioning devices on a macroscopic scale. For nano-physics, the narrow size distribution of aerosol-particle seeded nanowires has proved valuable, especially in the sub-50 nm range where alternative patterning methods have been difficult with respect to reproducibility. For devices, aerosol-seeded nanowires have been essential for fundamental technology development, but for some applications other patterning methods (e.g. NIL) have eventually yielded better results, cf. Section 5.4.

The ability to controllably grow thin axial heterostructures [63, 65], using Au aerosol particles to induce growth, was the starting point of advanced quantum devices in nanowires. It was demonstrated that a segment of InP in an InAs nanowire gives a conduction band offset of more than 600 meV, which is a substantial barrier for electrons. This was later used to show that by controlling the InP segment thickness from several tens of nanometers down to just a few nanometers, the tunnel currents flowing through the barrier could be varied over ten orders of magnitude, cf. Fig. 15 [118]. The addition of a second equally wide barrier separated from the first by an InAs quantum dot (10 nm wide InAs segment) resulted in the first demonstration of resonant electron tunneling through a quantum dot located inside a one-dimensional system. A clear sign of the quantized states in the InAs dot was observed as regions of negative differential resistance. Those devices typically had peak-to-valley current ratios of 10:1 but could measure as high as 50:1 – a telltale of the high hetero-interface quality in that system. The resonant tunneling diode just described was the first demonstration of transport through a one-dimensional quantum dot [119, 120].

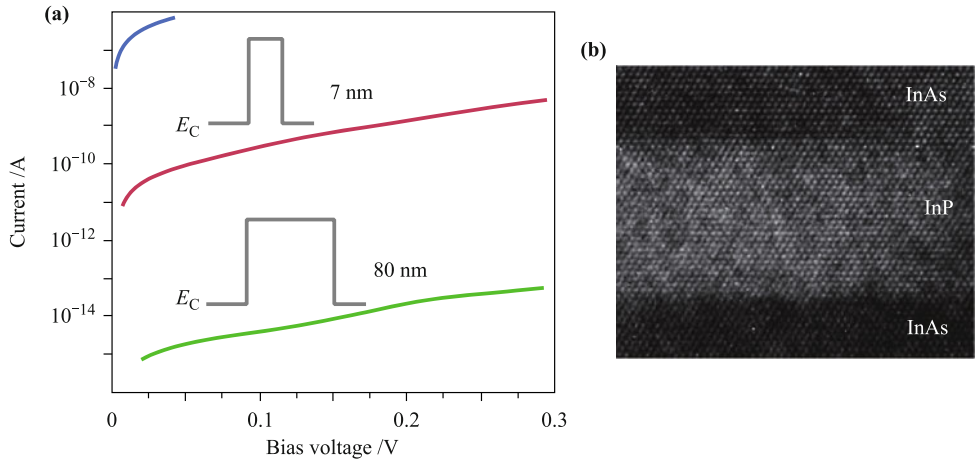

Fig. 15 Evaluation of transport mechanisms for InAs nanowires with single InP barriers of various thicknesses. **(a)** The current–voltage characteristics for three different barrier situations; the green curve shows data for an 80 nm barrier, the red curve for a 7 nm barrier and the blue curve for a reference sample with no barrier. **(b)** TEM image of an InAs nanowire with an 8 nm wide InP segment perpendicular to the long axis of the wire (Ref. [118]).

Subsequently, focus was put on scaling the quantum dot to learn more about the physics in the InAs/InP system. By using large dots (lengths of 100 nm) where the energy level spacing is smaller than the Coulomb charging energy in the system, single electron transistors where produced with classical Coulomb blockade effects (periodic Coulomb oscillations as a function of gate voltage). At a dot length of around 30 nm the energy level spacing at the Fermi energy starts to become equal to the charging energy and the Coulomb peaks start to form groups of twos and fours due to spin and orbital degeneracies in the quantum dot. In addition, the peak heights start to vary a lot, which is a clear sign of tunneling through discrete energy states. As the dot length is made only 10 nm long, the axial quantization is strong enough that the energy level spacing can be larger than the charging energy and so strong that the lowest bound state in the dot now lies above the Fermi level. The latter implies that the quantum dot is completely empty of electrons at zero gate potential. As the gate voltage is increased it is possible to track the addition of single electrons, one by one. In this case there is no periodicity left in the Coulomb oscillations but instead one can observe a clear shell structure in the filling of the quantum dot energy states as a function of gate voltage, cf. Fig. 16 [121]. The filling sequence of the dots was observed to be 2 electrons in the first shell, 4 in the second, 2 in the third, etc. forming the magic numbers 2, 6, 8, $\cdots$. The shell structure could be monitored up to adding roughly 50 electrons maintaining a constant charging energy indicating a rigid confinement potential (set by the heterostructure confinement in the axial direction and the wire cross section in the radial direction). This system of single quantum dots was further studied using magneto-transport where it was shown that the electron g-factor in the InAs quantum dots decreases from the bulk value

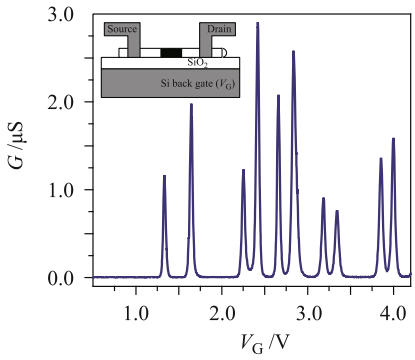

Fig. 16 Gate characteristics at 4.2 K of a single electron transistor with a 10 nm long dot, resulting in a device depleted of electrons at zero gate voltage. By increasing the electrostatic potential electrons are added one by one. For some electron configurations the addition energy is larger corresponding to filled electron shells (Ref. [121]).

at large dots to around 2 for very small dots [122] due to the increase in confinement, in accordance with theoretical predictions. A step further in complexity was demonstrated by Fuhrer *et al.* who added a second InAs quantum dot to the system giving a system of two coupled few-electron dots [123]. In the few-electron regime, starting with both dots empty, the low-temperature transport measurements reveal a clear shell structure in agreement with the single dot system for sequential charging of the larger of the two dots with up to 12 electrons. The resonant current through the double dot is found to depend on the orbital coupling between states of different radial symmetry. Furthermore, the charging energies are well described by a capacitance model if next-neighbor capacitances are taken into account.

The single and double quantum dot systems described so far can be controlled to very tight dimensions by growth and has proven to yield very rigid confinement potentials. A drawback with these systems is just that, it is hard to tune the confinement potentials and especially the interaction potential between two dots in the coupled systems. To that end, effort on making tunable InAs dots inside nanowires was pursued. By using a pure InAs nanowire and adding electrostatic gates on top of the wire, it was shown that quantum dots could be induced by using the gates to deplete the wire of charge locally, thus forming tunnel barriers. By applying a periodic pulse sequence to two plunger gate electrodes controlling the double quantum dot charge configuration, the device is operated as a single electron pump [124]. It was found that within measurement accuracy, the pumping current equals one electron per cycle for frequencies up to 2 MHz, demonstrating the suitability of nanowire based quantum dots for pumping applications. It was further demonstrated that using electrostatic gates it was even possible to control the electron number down to the last electron [125]. Using low temperature transport spectroscopy in the Coulomb blockade regime, it was possible to directly determine the magnitude of the spin–orbit interaction in a two-electron artificial atom with strong spin–orbit coupling to 127 nm.

InP nanowires grown from randomly positioned Au aerosol particles provided the first demonstration of how mixed crystal structures in nanowires may lead to internal type-II-like hetero-interfaces in which electrons are confined in zincblende-rich segments and holes in wurtzite-rich segments, with spatially indirect recombination occurring, cf. Fig. 17 [126]. These types of phenomena have later been labeled "Crystal Phase Quantum Dots" [127].

In the electrostatically gated quantum dots a strong interplay between the confined electronic and phononic

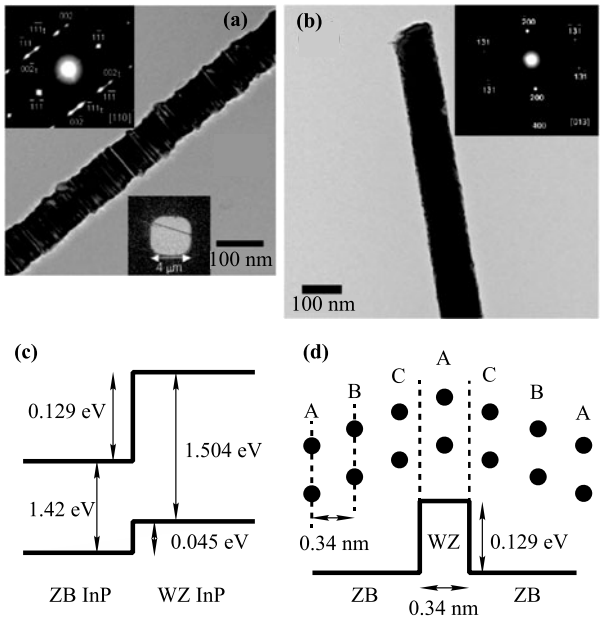

Fig. 17 **(a)** TEM image of an InP nanowire with rotational twinning. *Bottom inset*: An InP nanowire on an SiN membrane with both ends covered by Ti/Au film. *Top inset*: TEM diffraction pattern (DP) recorded along the [110] zone axis, revealing that a twinning zincblende (ZB) wire grown along the ⟨111⟩ direction. **(b)** TEM image of a single crystal ZB InP nanowire; the TEM diffraction pattern recorded along the [013] zone axis (inset) reveals that the wire is single crystal (no twin planes) and the growth direction is ⟨001⟩. **(c)** Band alignment between ZB InP and wurtzite (WZ) InP. **(d)** Conduction band potential profile and the corresponding thickness of WZ and ZB layers near a twin plane used for modeling the optical properties of a twinned wire. The CAC stacking is one unit of WZ InP; however, because the left layer C also belongs to the left BCA stacking (ZB), the right layer C belongs to the right ACB layer (ZB), so the effective thickness of WZ section is half of the thickness of CAC layer, which is ∼ 0.34 nm (Ref. [126]).

systems was found. Current spectroscopy in the few-electron regime of a nanowire-based double quantum dot made it possible to probe the confined phonon environment of the nanowire. The characteristic peak structure could be well explained theoretically if the piezoelectric coupling mechanism was taken into account [128].

5.4 Nanowire-based devices

The primary research area for nanowire-based devices grown from aerosol seed particles has been in electronics, especially for wrap-gate controlled nanowire transistors, and for optoelectronics, especially light emitting diodes (LEDs) and photovoltaics (PV). A high control with respect to particle size and particle density is necessary, not only to fulfill the device applications, but, primarily, to enable homogeneous growth of all separate axial and radial device layers within the ensemble of nanowire devices. Controlled deposition of seed particles over large areas as fulfilled by aerosol particle deposition is necessary (in addition to control over nanowire growth parameters), for growth of homogeneous nanowire device layers.

The fundamental studies of electronic transport in narrow nanowires, for instance of InAs, gave indications that it would be possible to design optimal field-effect transistor devices with the use of a thin dielectric surrounding the nanowire channel, again surrounded by a finite length metallic gate, which was developed in collaboration between leading European groups. For a review of this field of research, see Refs. [129] and [130].

The first nanowire red LEDs were grown monolithically on Si and GaP substrates. They were realized using 60 nm diameter Au aerosol particles with a mean particle density of 1 μm^{-2} [69–71, 131–134]. These light emitting diodes were of radial design with an n-type GaInP shell, selectively grown around an undoped GaAs core, the nanowire core being used as the light-emitting layer, cf. Fig. 18. This geometry is promising for further development due to the large interface area offered by the

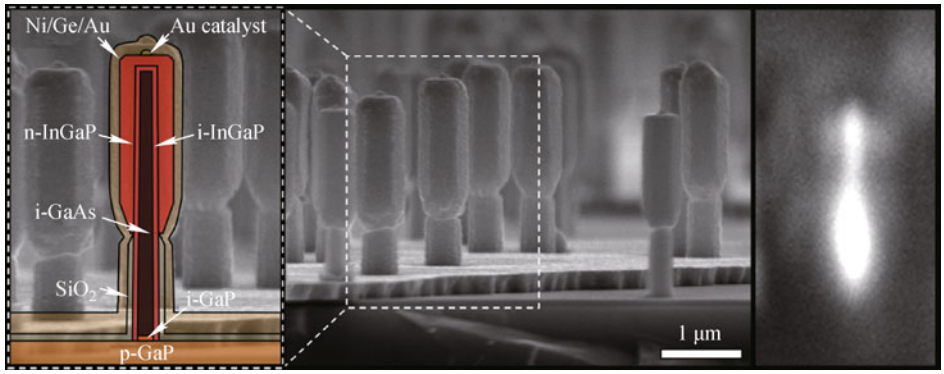

Fig. 18 Side-view SEM image showing nanowire light emitting diodes (LEDs) monolithically grown on a silicon wafer. The edge of the top contact layer is visible, and both the contacted and non-contacted LEDs can be seen. *Left inset*: Sketch drawing of the device structure. *Right inset*: Side-view CCD camera image showing electroluminescence (EL) from a single nanowire LED. The sample was cleaved and mounted in an optical microscopy set-up equipped with electrical probes allowing the study of an individual nanowire (Ref. [131]).

radial design where the pn-junction extends along the nanowires, and the freedom in tuning the shape of the nanowires such that the optical and electrical properties of the wires can be tuned individually.

Radial core-shell geometry in nano- or microwires has been identified as beneficial for solar energy harvesting since the radial configuration allows short diffusion lengths before carrier collection [135]. At the same time, the axial geometry has been assumed to suffer from poor absorption in sub-wavelength nanowire dimensions as well as from carrier losses due to the high surface-to-volume ratios dominated by surface recombination. However, the reduced sensitivity to lattice mismatch and thermal expansion due to strain relaxation in axial nanostructures leads to less complicated growth schemes and the freedom to design multi-junctions [94]. In collaboration between leading European groups, axial tandem junction solar cells were pursued, creating the first axially defined single band gap InP nanowire solar cells, seeded by aerosol particles, cf. Fig. 19 [94]. By use of *in situ* etching for eliminating radial growth and nanowire doping optimization, InP-based nanowire tandem junctions grown on a Si substrate were demonstrated [136–138]. The tandem junction operation was confirmed by open circuit voltage (V_{oc}) addition measured in single nanowires, with a V_{oc} of 1.4 V under intense illumination, cf. Fig. 19. The dual junction V_{oc} increased by only 67% compared to a single junction, limited mainly by series resistance over the non-ideal Esaki diode connecting the two photodiodes.

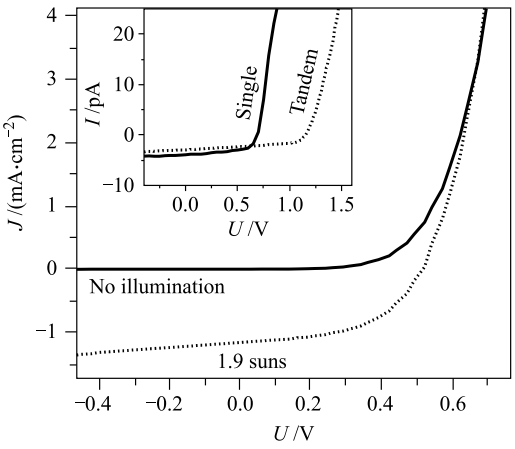

Fig. 19 Current–voltage characteristics of photovoltaic devices made from InP nanowires grown directly on Si from Au aerosol seed particles. The larger graph shows the response from a 300×300 μm^2 solar cell made from an array of nanowires with single pn-junctions in the dark and under approximately 1.9 sun illumination (Ref. [94]). The inset shows the response from two individual nanowires contacted laterally, illuminated with a green laser. One wire incorporates a single pn-junction, while the other contains two junctions connected in series by a tunnel diode, yielding an open circuit voltage greater than the InP bandgap, due to addition of the voltages from from the two sub-cells (Ref. [136]).

Modeling of light absorption in nanowire arrays made it clear that the aerosol particles (available up to 100 nm diameter) resulted in nanowires too thin for ideal optical absorption [139]. By moving to NIL for the seed particle definition, the degree of control over pitch and diameter definition increased significantly, at the expense of flexibility and simplicity. Using arrays of axial p–i–n InP nanowires with a diameter of 180 nm and a pitch of 470 nm, 1 mm^2 PV devices were made containing about 4 million nanowires each, with an efficiency of 13.8%, and with a short circuit current only 17% below that of the record planar InP cell [140]. This is seven times higher than what would be expected from simple ray optics, even though the nanowires only have 12% surface coverage. Modeling shows, however, that the solar cells require only short range order to reach high efficiencies, and therefore the aerosol route is still very promising for mass production, either for MOVPE-grown nanowires or for aerotaxy.

6 Summary and outlook

This review has collected a large variety of semiconductor nanostructures that have been realized by means of aerosol technology, in most cases benefiting from the opportunities to supply tightly size-selected and metallurgically designed nanoparticles. In a few cases the initial very strong influence of the technology may from now on be replaced by new and highly efficient fabrication methods, such as nano-imprint lithography, for example in microelectronic or LED applications. In other cases one can expect that the unique opportunities offered by the efficient supply of nanoparticles from the vapor phase will continue to generate new science and technology, for example in large-area solar cells.

Acknowledgements We would like to acknowledge first of all the many co-authors of the papers referenced in the review, and especially Hans-Christen Hansson and Alfred Wiedensohler for introducing us to aerosol technology; Reine Wallenberg and Jan-Olle Malm for advanced high-resolution TEM analysis; Claes Thelander for pioneering efforts in nanowire handling and characterization; and Andreas Fuhrer for developing technology for nanowire-based nano-physics.

Over the course of 20 years, we have been funded by several sources. We acknowledge support from the Swedish agencies NFR, STU, VINNOVA and from the Energy Agency; from Nordic Innovation; from the Foundation for Strategic Research (SSF) and Knut and Alice Wallenberg's Foundation (KAW); from the European Commission's ESPRIT project CHARGE (22953), FP6 project NODE (15783), and FP7 projects AMON-RA (214814) and BUONAPART-E (280765); from E.ON AG; and from the spin-off companies QuNano AB, Glo AB and Sol Voltaics AB.

References and notes

1. R. Mueller, L. Mädler, and S. E. Pratsinis, Nanoparticle synthesis at high production rates by flame spray pyrolysis, *Chem. Eng. Sci.*, 2003, 58(10): 1969
2. H. G. Craighead, 10-nm resolution electron-beam lithography, *J. Appl. Phys.*, 1984, 55(12): 4430
3. G. M. Whitesides, J. P. Mathias, and C. T. Seto, Molecular self-assembly and nanochemistry: A chemical strategy for the synthesis of nanostructures, *Science*, 1991, 254(5036): 1312
4. A. R. Kortan, R. Hull, R. L. Opila, M. G. Bawendi, M. L. Steigerwald, P. J. Carroll, and L. E. Brus, Nucleation and growth of cadmium selendie on zinc sulfide quantum crystallite seeds, and vice versa, in inverse micelle media, *J. Am. Chem. Soc.*, 1990, 112(4): 1327
5. W. Seifert, N. Carlsson, M. Miller, M. E. Pistol, L. Samuelson, and L. R. Wallenberg, In-situ growth of quantum dot structures by the Stranski-Krastanow growth mode, *Prog. Cryst. Growth Charact. Mater.*, 1996, 33(4): 423
6. H. Schift, Nanoimprint lithography: An old story in modern times? A review, *J. Vac. Sci. Technol. B*, 2008, 26(2): 458
7. W. C. Hinds, Aerosol Technology: Properties, Behavior, and Measurement of Airborne Particles, John Wiley & Sons, 2012
8. J. H. Vincent, Aerosol Sampling: Science, Standards, Instrumentation and Applications, John Wiley & Sons, 2007
9. R. C. Flagan, History of electrical aerosol measurements, *Aerosol Sci. Technol.*, 1998, 28(4): 301
10. P. Kulkarni, P. A. Baron, and K. Willeke (Eds.), Aerosol Measurement: Principles, Techniques, and Applications, John Wiley & Sons, 2011
11. S. E. Pratsinis, Flame aerosol synthesis of ceramic powders, *Pror. Energy Combust. Sci.*, 1998, 24(3): 197
12. M. Attoui, M. Paragano, J. Cuevas, and J. Fernandez de la Mora, Tandem DMA generation of strictly monomobile 1-3.5 nm particle standards, *Aerosol Sci. Technol.*, 2013, 47(5): 499
13. D. R. Chen, D. Y. H. Pui, G. W. Mulholland, and M. Fernandez, Design and testing of an aerosol/sheath inlet for high resolution measurements with a DMA, *J. Aerosol Sci.*, 1999, 30(8): 983
14. T. J. Krinke, H. Fissan, K. Deppert, M. H. Magnusson, and L. Samuelson, Positioning of nanometer-sized particles on flat surfaces by direct deposition from the gas phase, *Appl. Phys. Lett.*, 2001, 78(23): 3708
15. H. Kim, J. Kim, H. Yang, J. Suh, T. Kim, B. Han, S. Kim, D. S. Kim, P. V. Pikhitsa, and M. Choi, Parallel patterning of nanoparticles via electrodynamic focusing of charged aerosols, *Nat. Nanotechnol.*, 2006, 1(2): 117
16. L. Qi, P. H. McMurry, D. J. Norris, and S. L. Girshick, Micropattern deposition of colloidal semiconductor nanocrystals by aerodynamic focusing, *Aerosol Sci. Technol.*, 2010, 44(1): 55
17. S. H. Kim, G. W. Mulholland, and M. R. Zachariah, Understanding ion-mobility and transport properties of aerosol nanowires, *J. Aerosol Sci.*, 2007, 38(8): 823
18. K. Ehara, C. Hagwood, and K. J. Coakley, Novel method to classify aerosol particles according to their mass-to-charge ratio – Aerosol particle mass analyser, *J. Aerosol Sci.*, 1996, 27(2): 217
19. H. G. Scheibel and J. Porstendörfer, Generation of monodisperse Ag- and NaCl-aerosols with particle diameters between 2 and 300 nm, *J. Aerosol Sci.*, 1983, 14(2): 113
20. B. Y. H. Liu and D. Y. H. Pui, Electrical neutralization of aerosols, *J. Aerosol Sci.*, 1974, 5(5): 465
21. E. O. Knutson and K. T. Whitby, Aerosol classification by electric mobility: Apparatus, theory, and applications, *J. Aerosol Sci.*, 1975, 6(6): 443
22. M. N. A. Karlsson, K. Deppert, L. S. Karlsson, M. H. Magnusson, J. O. Malm, and N. S. Srinivasan, Compaction of agglomerates of aerosol nanoparticles: A compilation of experimental data, *J. Nanopart. Res.*, 2005, 7(1): 43
23. M. H. Magnusson, K. Deppert, J. O. Malm, J. O. Bovin, and L. Samuelson, Gold nanoparticles: Production, reshaping, and thermal charging, *J. Nanopart. Res.*, 1999, 1(2): 243
24. M. H. Magnusson, K. Deppert, and J. O. Malm, Single-crystalline tungsten nanoparticles produced by thermal decomposition of tungsten hexacarbonyl, *J. Mater. Res.*, 2000, 15(07): 1564
25. M. L. Ostraat, J. W. De Blauwe, M. L. Green, L. D. Bell, M. L. Brongersma, J. Casperson, R. C. Flagan, and H. A. Atwater, Synthesis and characterization of aerosol silicon nanocrystal nonvolatile floating-gate memory devices, *Appl. Phys. Lett.*, 2001, 79(3): 433
26. S. Schwyn, E. Garwin, and A. Schmidt-Ott, Aerosol generation by spark discharge, *J. Aerosol Sci.*, 1988, 19(5): 639
27. B. O. Meuller, M. E. Messing, D. L. J. Engberg, A. M. Jansson, L. I. M. Johansson, S. M. Norlén, N. Tureson, and K. Deppert, Review of spark discharge generators for production of nanoparticle aerosols, *Aerosol Sci. Technol.*, 2012, 46(11): 1256
28. N. S. Tabrizi, Q. Xu, N. M. van der Pers, and A. Schmidt-Ott, Generation of mixed metallic nanoparticles from immiscible metals by spark discharge, *J. Nanopart. Res.*, 2010, 12(1): 247
29. M. E. Messing, R. Westerström, B. O. Meuller, S. Blomberg, J. Gustafson, J. N. Andersen, E. Lundgren, R. van Rijn, O. Balmes, H. Bluhm, and K. Deppert, Generation of Pd model catalyst nanoparticles by spark discharge, *J. Phys. Chem. C*, 2010, 114(20): 9257
30. M. E. Messing, C. R. Svensson, J. Pagels, B. O. Meuller, K. Deppert, and J. Rissler, Gas-borne particles with tunable and highly controlled characteristics for nanotoxicology studies, *Nanotoxicology*, 2013, 7(6): 1052

31. T. V. Pfeiffer, P. Keijzer, and A. Schmidt-Ott, A controlled spark generator for increased nanoparticle production, Europ. Aerosol Conf., 16 Sep. 2013, Prague
32. E. Hontañón, J. M. Palomares, M. Stein, X. Guo, R. Engeln, H. Nirschl, and F. E. Kruis, Experimental study on the transition from spark to arc discharge with respect to nanoparticle production, Europ. Aerosol Conf., 16 Sep. 2013, Prague
33. R. P. Elliott and F. A. Shunk, The Au Ga (Gold Gallium) system, *Bull Alloy Phase Diagr.*, 1981, 2(3): 356
34. H. Okamoto and T. B. Massalski, The Au Si (Gold Silicon) system, *Bull Alloy Phase Diagr.*, 1983, 4(2): 190
35. M. N. A. Karlsson, K. Deppert, M. H. Magnusson, L. S. Karlsson, and J. O. Malm, Size- and composition-controlled Au-Ga aerosol nanoparticles, *Aerosol Sci. Technol.*, 2004, 38(9): 948
36. M. H. Magnusson, Metal and Semiconductor Nanocrystals for Quantum Devices, Lund University, 2001
37. A. Maisels, F. E. Kruis, and H. Fissan, Mixing selectivity in bicomponent, bipolar aggregation, *J. Aerosol Sci.*, 2002, 33(1): 35
38. K. Deppert and L. Samuelson, Self-limiting transformation of monodisperse Ga droplets into GaAs nanocrystals, *Appl. Phys. Lett.*, 1995, 68(10): 1409
39. K. Deppert, M. H. Magnusson, L. Samuelson, J. O. Malm, C. Svensson, and J. O. Bovin, Size-selected nanocrystals of III-V semiconductor materials by the aerotaxy method, *J. Aerosol Sci.*, 1998, 29(5–6): 737
40. K. Deppert, J. O. Bovin, M. H. Magnusson, J. O. Malm, C. Svensson, and L. Samuelson, Aerosol fabrication of nanocrystals of InP, *Jpn. J. Appl. Phys.*, 1999, 38: 1056
41. N. Anttu and H. Q. Xu, Coupling of light into nanowire arrays and subsequent absorption, *J. Nanosci. Technol.*, 2010, 10(11): 7183
42. X. Duan, J. Wang, and C. M. Lieber, Synthesis and optical properties of gallium arsenide nanowires, *Appl. Phys. Lett.*, 2000, 76(9): 1116
43. X. Duan, Y. Huang, Y. Cui, J. Wang, and C. M. Lieber, Indium phosphide nanowires as building blocks for nanoscale electronic and optoelectronic devices, *Nature*, 2001, 409(6816): 66
44. A. A. Guzelian, J. E. B. Katari, A. V. Kadavanich, U. Banin, K. Hamad, E. Juban, A. P. Alivisatos, R. H. Wolters, C. C. Arnold, and J. R. Heath, Synthesis of size-selected, surface-passivated InP nanocrystals, *J. Phys. Chem.*, 1996, 100(17): 7212
45. M. Heurlin, M. H. Magnusson, D. Lindgren, M. Ek, L. R. Wallenberg, K. Deppert, and L. Samuelson, Continuous gas-phase synthesis of nanowires with tunable properties, *Nature*, 2012, 492(7427): 90
46. S. H. Kim and M. R. Zachariah, Gas-phase growth of diameter-controlled carbon nanotubes, *Mater. Lett.*, 2007, 61(10): 2079
47. U. Krishnamachari, M. Borgström, B. J. Ohlsson, N. Panev, L. Samuelson, W. Seifert, M. W. Larsson, and L. R. Wallenberg, Defect-free InP nanowires grown in [001] direction on InP (001), *Appl. Phys. Lett.*, 2004, 85(11): 2077
48. To be published separately.
49. L. Samuelson, M. Heurlin, M. Magnusson, and K. Deppert, PCT patent application, 2011, WO/2011/142717
50. A. Wiedensohler, H. C. Hansson, I. Maximov, and L. Samuelson, Nanometer patterning of InP using aerosol and plasma etching techniques, *Appl. Phys. Lett.*, 1992, 61(7): 837
51. I. Maximov, A. Gustafsson, H. C. Hansson, L. Samuelson, W. Seifert, and A. Wiedensohler, Fabrication of quantum dot structures using aerosol deposition and plasma etching techniques, *J. Vac. Sci. Technol.*, 1993, 11(4): 748
52. K. Deppert, I. Maximov, L. Samuelson, H. C. Hansson, and A. Wiedensohler, Sintered aerosol masks for dry-etched quantum dots, *Appl. Phys. Lett.*, 1994, 64(24): 3293
53. I. Maximov, K. Deppert, L. Montelius, L. Samuelson, S. Gray, M. Johansson, H. C. Hansson, and A. Wiedensohler, Characterization of InP/GaInAs nanometer sized columns produced by aerosol deposition and plasma etching, *Mat. Res. Soc. Symp. Proc.*, 1994, 332: 513
54. I. Maximov, E.-L. Sarwe, M. Beck, K. Deppert, M. Graczyk, M. H. Magnusson, and L. Montelius, Fabrication of Si-based nanoimprint stamps with sub-20 nm features, *Microelectr. Eng.*, 2002, 61–62: 449
55. B. A. Wacaser, K. A. Dick, Z. Zanolli, A. Gustafsson, K. Deppert, and L. Samuelson, Size-selected compound semiconductor quantum dots by nanoparticle conversion, *Nanotechnology*, 2007, 18(10): 105306
56. K. Watanabe, N. Koguchi, and Y. Gotoh, Fabrication of GaAs quantum dots by modified droplet epitaxy, *Jpn. J. Appl. Phys.*, 2000, 39: L79
57. R. S. Wagner and W. C. Ellis, Vapor-liquid-solid mechanism of single crystal growth, *Appl. Phys. Lett.*, 1964, 4(5): 89
58. E. I. Givargizov, Fundamental aspects of VLS growth, *J. Cryst. Growth*, 1975, 31: 20
59. M. Yazawa, M. Koguchi, and K. Hiruma, Heteroepitaxial ultrafine wire-like growth of InAs on GaAs substrates, *Appl. Phys. Lett.*, 1991, 58(10): 1080
60. K. A. Dick, A review of nanowire growth promoted by alloys and non-alloying elements with emphasis on Au-assisted III-V nanowires, *Prog. Cryst. Growth Charact. Mater.*, 2009, 54(3-4): 138
61. M. E. Messing, K. Hillerich, J. Bolinsson, K. Storm, J. Johansson, K. A. Dick, and K. Deppert, A comparative study of the effect of gold seed particle preparation method on nanowire growth, *Nano Res.*, 2010, 3(7): 506
62. B. J. Ohlsson, M. T. Björk, M. H. Magnusson, K. Deppert, L. Samuelson, and L. R. Wallenberg, Size-, shape-, and position-controlled GaAs nano-whiskers, *Appl. Phys. Lett.*, 2001, 79(20): 3335

63. M. T. Björk, B. J. Ohlsson, T. Sass, A. I. Persson, C. Thelander, M. H. Magnusson, K. Deppert, L. R. Wallenberg, and L. Samuelson, One-dimensional heterostructures in semiconductor nano-whiskers, *Appl. Phys. Lett.*, 2002, 80(6): 1058
64. M. T. Björk, B. J. Ohlsson, T. Sass, A. I. Persson, C. Thelander, M. H. Magnusson, K. Deppert, L. R. Wallenberg, and L. Samuelson, One-dimensional steeplechase for electrons realized, *Nano Lett.*, 2002, 2(2): 87
65. L. I. Samuelson and B. J. Ohlsson, United States patent, 2003, US 7,335,908
66. L. E. Fröberg, B. A. Wacaser, J. B. Wagner, S. Jeppesen, B. J. Ohlsson, K. Deppert, and L. Samuelson, Transients in the formation of nanowire heterostructures, *Nano Lett.*, 2008, 8(11): 3815
67. B. J. Ohlsson, M. T. Björk, A. I. Persson, C. Thelander, L. R. Wallenberg, M. H. Magnusson, K. Deppert, and L. Samuelson, Growth and characterization of GaAs and InAs nano-whiskers and InAs/GaAs heterostructures, *Physica E*, 2002, 13(2–4): 1126
68. T. Mårtensson, C. P. T. Svensson, B. A. Wacaser, M. W. Larsson, W. Seifert, K. Deppert, A. Gustafsson, L. R. Wallenberg, and L. Samuelson, Epitaxial III–V nanowires on silicon, *Nano Lett.*, 2004, 4(10): 1987
69. L. I. Samuelson and T. M. I. Mårtensson, United States patent, 2009, US 7,528,002
70. L. I. Samuelson and T. M. I. Mårtensson, United States patent, 2011, US 7,960,260
71. L. Samuelson, J. Ohlsson, T. Mårtensson, and P. Svensson, United States patent, 2011, US 8,084,337
72. A. I. Persson, M. W. Larsson, S. Stenström, B. J. Ohlsson, L. Samuelson, and L. R. Wallenberg, Solid-phase diffusion mechanism for GaAs nanowire growth, *Nat. Mater.*, 2004, 3(10): 677
73. J. Johansson, C. P. T. Svensson, T. Mårtensson, L. Samuelson, and W. Seifert, Mass transport model for semiconductor nanowire growth, *J. Phys. Chem. B*, 2005, 109(28): 13567
74. L. E. Fröberg, W. Seifert, and J. Johansson, Diameter-dependent growth rate of InAs nanowires, *Phys. Rev. B*, 2007, 76(15): 153401
75. P. Caroff, K. A. Dick, J. Johansson, M. E. Messing, K. Deppert, and L. Samuelson, Controlled polytypic and twin-plane superlattices in III–V nanowires, *Nat. Nanotechnol.*, 2009, 4(1): 50
76. J. Johansson, K. A. Dick, P. Caroff, M. E. Messing, J. Bolinsson, K. Deppert, and L. Samuelson, Diameter dependence of the wurtzite-zinc blende transition in InAs nanowires, *J. Phys. Chem. C*, 2010, 114(9): 3837
77. K. A. Dick, J. Bolinsson, B. M. Borg, and J. Johansson, Controlling the abruptness of axial heterojunctions in III–V nanowires: Beyond the reservoir effect, *Nano Lett.*, 2012, 12(6): 3200
78. M. Ek, B. M. Borg, J. Johansson, and K. A. Dick, Diameter limitation in growth of III-Sb-containing nanowire heterostructures, *ACS Nano*, 2013, 7(4): 3668
79. M. A. Verheijen, G. Immink, T. de Smet, M. T. Borgström, and E. P. A. M. Bakkers, Growth kinetics of heterostructured GaP-GaAs nanowires, J. Am. Chem. Soc., 2006, 128(4): 1353
80. H. J. Joyce, Q. Gao, H. H. Tan, C. Jagadish, Y. Kim, X. Zhang, Y. N. Guo, and J. Zou, Twin-free uniform epitaxial GaAs nanowires grown by a two-temperature process, *Nano Lett.*, 2007, 7(4): 921
81. L. J. Lauhon, M. S. Gudiksen, D. Wang, and C. M. Lieber, Epitaxial core-shell and core-multishell nanowire heterostructures, *Nature*, 2002, 420(6911): 57
82. H. J. Joyce, Q. Gao, H. H. Tan, C. Jagadish, Y. Kim, M. A. Fickenscher, S. Perera, T. B. Hoang, L. M. Smith, H. E. Jackson, J. M. Yarrison-Rice, X. Zhang, and J. Zou, Unexpected benefits of rapid growth rate for III–V nanowires, *Nano Lett.*, 2009, 9(2): 695
83. M. Suhara, C. Nagao, H. Honji, Y. Miyamoto, K. Furuya, and R. Takemura, Atomically flat OMVPE growth of GaInAs and InP observed by AFM for level narrowing in resonant tunneling diodes, *J. Cryst. Growth*, 1997, 179(1–2): 18
84. G. B. Stringfellow, Organometallic Vapor Phase Epitaxy, 2nd Ed., San Diego: Academic Press, 1999
85. M. T. Borgström, J. Wallentin, J. Trägårdh, P. Ramvall, M. Ek, L. R. Wallenberg, L. Samuelson, and K. Deppert, In Situ etching for total control over axial and radial nanowire growth, *Nano Res.*, 2010, 3(4): 264
86. J. Wallentin, M. E. Messing, E. Trygg, L. Samuelson, K. Deppert, and M. T. Borgström, Growth of doped $InAs_yP_{1-y}$ nanowires with InP shells, *J. Cryst. Growth*, 2011, 331(1): 8
87. D. Jacobsson, J. M. Persson, D. Kriegner, T. Etzelstorfer, J. Wallentin, J. B. Wagner, J. Stangl, L. Samuelson, K. Deppert, and M. T. Borgström, Particle-assisted $Ga_xIn_{1-x}P$ nanowire growth for designed bandgap structures, *Nanotechnology*, 2012, 23(24): 245601
88. J. Wallentin, J. M. Persson, J. B. Wagner, L. Samuelson, K. Deppert, and M. T. Borgström, High-performance single nanowire tunnel diodes, *Nano Lett.*, 2010, 10(3): 974
89. M. T. Borgström, J. Wallentin, K. Kawaguchi, L. Samuelson, and K. Deppert, Dynamics of extremely anisotropic etching of InP nanowires by HCl, *Chem. Phys. Lett.*, 2011, 502(4–6): 222
90. G. L. Tuin, M. T. Borgström, J. Trägårdh, M. Ek, L. R. Wallenberg, L. Samuelson, and M. E. Pistol, Valence band splitting in wurtzite InP nanowires observed by photoluminescence and photoluminescence excitation spectroscopy, *Nano Res.*, 2011, 4(2): 159
91. J. Wallentin, P. Wickert, M. Ek, A. Gustafsson, L. R. Wallenberg, M. H. Magnusson, L. Samuelson, K. Deppert, and M. T. Borgström, Degenerate p-doping of InP nanowires for large area tunnel diodes, *Appl. Phys. Lett.*, 2011, 99(25): 253015

92. J. Wallentin and M. T. Borgström, Doping of semiconductor nanowires, *J. Mater. Res.*, 2011, 26(17): 2142
93. J. Eskola, J. A. Seetula, and R. S. Timonen, Kinetics of the CH_3+HCl/DCl → CH_4/CH_3D+Cl and CD_3+HCl/DCl → CD_3H/CD_4+Cl reactions: An experimental H atom tunneling investigation, *Chem. Phys.*, 2006, 331(1): 26
94. M. T. Borgström, J. Wallentin, M. Heurlin, S. Fält, P. Wickert, J. Leene, M. H. Magnusson, K. Deppert, and L. Samuelson, Nanowires with promise for photovoltaics, *IEEE J. Sel. Top. Quantum Electron.*, 2011, 17(4): 1050
95. K. A. Dick, K. Deppert, L. S. Karlsson, M. W. Larsson, W. Seifert, L. R. Wallenberg, and L. Samuelson, Directed growth of branched nanowire structures, *MRS Bull.*, 2007, 32(02): 127
96. K. A. Dick, K. Deppert, M. W. Larsson, T. Mårtensson, W. Seifert, L. R. Wallenberg, and L. Samuelson, Synthesis of branched "nanotrees" by controlled seeding of multiple branching events, *Nat. Mater.*, 2004, 3(6): 380
97. L. I. Samuelson and K. W. Deppert, United States patent, 2010, US 7,662,706
98. L. I. Samuelson and K. W. Deppert, United States patent, 2010, US 7,875,536
99. K. Bayer, K. A. Dick, T. J. Krinke, and K. Deppert, Targeted deposition of Au aerosol nanoparticles on vertical nanowires for the creation of nanotrees, *J. Nanopart. Res.*, 2007, 9(6): 1211
100. K. A. Dick, K. Deppert, M. W. Larsson, W. Seifert, L. Reine Wallenberg, and L. Samuelson, Height-controlled nanowire branches on nanotrees using a polymer mask, *Nanotechnology*, 2007, 18(3): 035601
101. K. A. Dick, K. Deppert, L. S. Karlsson, W. Seifert, L. R. Wallenberg, and L. Samuelson, Position-controlled interconnected InAs nanowire networks, *Nano Lett.*, 2006, 6(12): 2842
102. K. A. Dick, Z. Geretovszky, A. Mikkelsen, L. S. Karlsson, E. Lundgren, J. O. Malm, J. N. Andersen, L. Samuelson, W. Seifert, B. A. Wacaser, and K. Deppert, Improving InAs nanotree growth with composition-controlled Au-In nanoparticles, *Nanotechnology*, 2006, 17(5): 1344
103. T. Junno, S. Anand, K. Deppert, L. Montelius, and L. Samuelson, Contact mode atomic force microscopy imaging of nanometer-sized particles, *Appl. Phys. Lett.*, 1995, 66(24): 3295
104. T. Junno, K. Deppert, L. Montelius, and L. Samuelson, Controlled manipulation of nanoparticles with an atomic force microscope, *Appl. Phys. Lett.*, 1995, 66(26): 3627
105. T. Junno, S. B. Carlsson, H. Q. Xu, L. Montelius, and L. Samuelson, Fabrication of quantum devices by angstrom-level manipulation of nanoparticles with an atomic force microscope, *Appl. Phys. Lett.*, 1998, 72: 548
106. T. Junno, M. H. Magnusson, S. B. Carlsson, K. Deppert, J. O. Malm, L. Montelius, and L. Samuelson, Single-electron devices via controlled assembly of designed nanoparticles, *Microelectron. Eng.*, 1999, 47(1–4): 179
107. C. Thelander, M. H. Magnusson, and K. Deppert, L. Samuelson, P. R. Poulsen, J. Nygård, and J. Borggreen, Gold nanoparticle single-electron transistor with carbon nanotube leads, *Appl. Phys. Lett.*, 2001, 79: 2016
108. T. Junno, S. B. Carlsson, H. Q. Xu, L. Samuelson, A. O. Orlov, and G. L. Snider, Single-electron tunneling effects in a metallic double dot device, *Appl. Phys. Lett.*, 2002, 80(4): 667
109. L. I. Samuelson and K. W. Deppert, United States patent, 2004, US 6,744,065
110. S. K. Lee, C. M. Zetterling, M. Östling, I. Åberg, M. H. Magnusson, K. Deppert, L. E. Wernersson, L. Samuelson, and A. Litwin, Reduction of the Schottky barrier height on silicon carbide using Au nano-particles, *Solid-State Electron.*, 2002, 46(9): 1433
111. L. E. Wernersson, A. Litwin, L. Samuelson, and W. Seifert, Controlled Carrier Depletion around Nano-Scale Metal Discs Embedded in GaAs, *Jpn. J. Appl. Phys.*, 1997, 36: L1628
112. L. E. Wernersson, A. Litwin, L. Samuelson, and H. Xu, Operation of a ballistic heterojunction permeable base transistor, *IEEE Trans. Electron. Dev.*, 1997, 44(11): 1829
113. L. E. Wernersson, M. Borgström, B. Gustafson, A. Gustafsson, L. Jarlskog, J. O. Malm, A. Litwin, L. Samuelson, and W. Seifert, MOVPE overgrowth of metallic features for realisation of 3D metal-semiconductor quantum devices, *J. Cryst. Growth*, 2000, 221(1–4): 704
114. I. Åberg, K. Deppert, M. H. Magnusson, I. Pietzonka, W. Seifert, L. E. Wernersson, and L. Samuelson, Nanoscale tungsten aerosol particles embedded in GaAs, *Appl. Phys. Lett.*, 2002, 80(16): 2976
115. H. Fissan, M. K. Kennedy, T. J. Krinke, and F. E. Kruis, *J. Nanopart. Res.*, 2003, 5(3–4): 299
116. C. Busch, G. Schierning, R. Theissmann, A. Nedic, F. E. Kruis, and R. Schmechel, Thin-film transistors with a channel composed of semiconducting metal oxide nanoparticles deposited from the gas phase, *J. Nanopart. Res.*, 2012, 14(6): 888
117. K. W. Deppert, C. M. H. Magnusson, L. I. Samuelson, and T. J. Krinke, United States patent, 2007, US 7,223,444
118. M. T. Björk, B. J. Ohlsson, C. Thelander, A. I. Persson, K. Deppert, L. R. Wallenberg, and L. Samuelson, Nanowire resonant tunneling diodes, *Appl. Phys. Lett.*, 2002, 81(23): 4458
119. L. Samuelson, C. Thelander, M. T. Björk, M. Borgström, K. Deppert, K. A. Dick, A. E. Hansen, T. Mårtensson, N. Panev, A. I. Persson, W. Seifert, N. Sköld, M. W. Larsson, and L. R. Wallenberg, Semiconductor nanowires for 0D and 1D physics and applications, *Physica E*, 2004, 25(2–3): 313
120. C. Thelander, T. Mårtensson, M. T. Björk, B. J. Ohlsson, M. W. Larsson, L. R. Wallenberg, and L. Samuelson, Single-electron transistors in heterostructure nanowires, *Appl. Phys. Lett.*, 2003, 83(10): 2052
121. M. T. Björk, C. Thelander, A. E. Hansen, L. E. Jensen, M. W. Larsson, L. R. Wallenberg, and L. Samuelson, Few-

electron quantum dots in nanowires, *Nano Lett.*, 2004, 4(9): 1621

122. M. T. Björk, A. Fuhrer, A. E. Hansen, M. W. Larsson, L. E. Fröberg, and L. Samuelson, Tunable effective g factor in InAs nanowire quantum dots, *Phys. Rev. B*, 2005, 72(20): 201307
123. A. Fuhrer, L. E. Fröberg, J. N. Pedersen, M. W. Larsson, A. Wacker, M. E. Pistol, and L. Samuelson, Few electron double quantum dots in InAs/InP nanowire heterostructures, *Nano Lett.*, 2007, 7(2): 243
124. A. Fuhrer, C. Fasth, and L. Samuelson, Single electron pumping in InAs nanowire double quantum dots, *Appl. Phys. Lett.*, 2007, 91(5): 052109
125. C. Fasth, A. Fuhrer, L. Samuelson, V. N. Golovach, and D. Loss, Direct measurement of the spin–orbit interaction in a two-electron InAs nanowire quantum dot, *Phys. Rev. Lett.*, 2007, 98(26): 266801
126. J. Bao, D. C. Bell, F. Capasso, J. B. Wagner, T. Mårtensson, J. Trägårdh, and L. Samuelson, Optical properties of rotationally twinned InP nanowire heterostructures, *Nano Lett.*, 2008, 8(3): 836
127. N. Akopian, G. Patriarche, L. Liu, J. C. Harmand, and V. Zwiller, Crystal phase quantum dots, *Nano Lett.*, 2010, 10(4): 1198
128. C. Weber, A. Fuhrer, C. Fasth, G. Lindwall, L. Samuelson, and A. Wacker, Probing confined phonon modes by transport through a nanowire double quantum dot, *Phys. Rev. Lett.*, 2010, 104(3): 036801
129. C. Thelander, P. Agarwal, S. Brongersma, J. Eymery, L. F. Feiner, A. Forchel, M. Scheffler, W. Riess, B. J. Ohlsson, U. Gösele, and L. Samuelson, Nanowire-based one-dimensional electronics, *Mater. Today*, 2006, 9(10): 28
130. C. Thelander, C. Rehnstedt, L. E. Fröberg, E. Lind, T. Mårtensson, P. Caroff, T. Löwgren, B. J. Ohlsson, L. Samuelson, and L. E. Wernersson, Development of a vertical wrap-gated InAs FET, *IEEE Trans. Electron. Dev.*, 2008, 55(11): 3030
131. C. P. T. Svensson, T. Mårtensson, J. Trägårdh, C. Larsson, M. Rask, D. Hessman, L. Samuelson, and J. Ohlsson, Monolithic GaAs/InGaP nanowire light emitting diodes on silicon, *Nanotechnology*, 2008, 19(30): 305201
132. L. I. Samuelson, P. Svensson, J. Ohlsson, and T. Löwgren, United States patent, 2011, US 8,049,203
133. L. I. Samuelson, B. Pedersen, and B. J. Ohlsson, United States patent, 2012, US 8,183,587
134. B. Pedersen, L. Samuelson, J. Ohlsson, and P. Svensson, United States patent, 2012, US 8,227,817
135. B. M. Kayes, H. A. Atwater, and N. S. Lewis, Comparison of the device physics principles of planar and radial p-n junction nanorod solar cells, *J. Appl. Phys.*, 2005, 97(11): 114302
136. M. Heurlin, P. Wickert, S. Fält, M. T. Borgström, K. Deppert, L. Samuelson, and M. H. Magnusson, Axial InP nanowire tandem junction grown on a silicon substrate, *Nano Lett.*, 2011, 11(5): 2028
137. L. Samuelson, M. Magnusson, and F. Capasso, United States patent application, US 2010/0186809
138. M. Borgström, M. Heurlin, and S. Fält, United States patent application, US 2012/0199187
139. N. Anntu and H. Q. Xu, Coupling of light into nanowire arrays and subsequent absorption, *J. Nanosci. Nanotechnol.*, 2010, 10(11): 7183
140. J. Wallentin, N. Anttu, D. Asoli, M. Huffman, I. Åberg, M. H. Magnusson, G. Siefer, P. Fuss-Kailuweit, F. Dimroth, B. Witzigmann, H. Q. Xu, L. Samuelson, K. Deppert, and M. T. Borgström, InP nanowire array solar cells achieving 13.8% efficiency by exceeding the ray optics limit, *Science*, 2013, 339(6123): 1057